IEEE Access
Multidisciplinary ⋮ Rapid Review ⋮ Open Access Journal

Received 5 February 2024, accepted 1 April 2024, date of publication 4 April 2024, date of current version 3 June 2024.

Digital Object Identifier 10.1109/ACCESS.2024.3385089

RESEARCH ARTICLE

A New Scheme of Harris Hawk Optimizer With Memory Saving Strategy (HHO-MSS) for Controlling Parameters of Power System Stabilizer and Virtual Inertia in Renewable Microgrid Power System

MOHAMAD ALMAS PRAKASA[1], IMAM ROBANDI[1], RYO NISHIMURA[2], AND MUHAMMAD RUSWANDI DJALAL[1]

[1]Department of Electrical Engineering, Institut Teknologi Sepuluh Nopember, Surabaya 60111, Indonesia
[2]Department of Information and Electronics, Faculty of Engineering, Tottori University, Tottori 680-8552, Japan

Corresponding author: Imam Robandi (robandi@ee.its.ac.id)

This work was supported by the Directorate of Research, Technology, and Community Service (Direktorat Riset, Teknologi, dan Pengabdian kepada Masyarakat, DRPM), Ministry of Education, Culture, Research, and Technology (Kementerian Pendidikan, Kebudayaan, Riset dan Teknologi, Kemendikbudristek), Republic of Indonesia, under Grant 1248/PKS/ITS/2023.

ABSTRACT Renewable microgrid power systems confront a typical stability challenge due to the deficiency of damping and inertia properties. This stability can be maintained by controlling the parameters of the Power System Stabilizer (PSS) and Virtual Inertia (VI). This paper proposes a new approach for controlling the optimal parameters of PSS and VI in the renewable microgrid power system consisting of a conventional generator, Photovoltaic Energy System (PVES), Wind Turbine Energy System (WTES), and Battery Energy Storage System (BESS). A new scheme of Harris Hawk Optimizer with Memory Saving Strategy (HHO-MSS) is proposed as the robust optimizer. Benson Scalarization Technique is also introduced to combine objective functions dependent on the damping factor and damping ratio. Using the Friedman Ranking Test, superior performances in exploration and exploitation processes conducted by HHO-MSS over the other modified versions of HHO and basic algorithms. Moreover, significant improvements have been conducted by HHO-MSS, especially in the convergence curve characteristics and the proportion between exploration and exploitation processes. The fitness values that have been produced by HHO-MSS are 9% to 26% better than the other algorithms. The optimal parameters are investigated by eigenvalue and time domain analysis in low, mid, high, and full RES penetrations. In the low and mid RES penetration analysis, PSS has better stability improvements than VI. On the other hand, VI has better stability improvement than PSS in high and full RES penetration analysis. Besides that, the best stability improvements in all RES penetrations with optimal Rate of Change of Frequency (RoCoF) reduction, smallest overshoot, and smoothest frequency and power angle responses are established by the proposed approach that controlling the optimal parameters of PSS and VI by using HHO-MSS. Moreover, the performance indexes validation has justified the proposed approach has the highest average error reduction of 47.26% over the existing approaches.

INDEX TERMS Harris hawk optimizer, memory saving strategy, power system stabilizer, renewable microgrid, virtual inertia.

The associate editor coordinating the review of this manuscript and approving it for publication was Amin Mahmoudi.

NOMENCLATURE

A	swept area by the WT.
$C_{eq,pool}$	equilibrium pool.
C_P	power coefficient of WT.
CV	control variable.
D	damping properties.
D_{VI}	virtual damping constant.
E	escaping energy of the rabbit.
E_{b1}	maximum overvoltage in battery.
E_{boc}	open circuit voltage.
E_o	initial energy parameter of the rabbit.
E'_q	terminal voltage.
F	exponential factor.
f_1, f_2	objective function.
$f_{benson's}$	objective function in benson scalarization.
G	generation rate.
I_{O_BESS}	DC through BESS.
J	jump strength of the rabbit.
$k_1 - k_6$	dynamic behavior based on the Heffron-Phillips model.
k_A	amplifier's time constant.
K_b	gain constant in battery.
K_{PSS}	gain constant of PSS.
K_{PV}	gain constant of PVES.
K_{VI}	gain constant of VI.
L_B	lower bound.
LF	levy flight in HHO.
N_{HHO}	number of populations in HHO.
N_{PV}	power-rated of PV.
r_{b1}	overvoltage resistance.
R	solar GHI.
q	exploration phase determination in HHO.
r_{bp}	self-discharge resistance.
r_{bs}	internal resistance.
R_S	solar GHI in STC condition.
$T_1 - T_4$	tunable parameters of PSS.
T	ambient temperature.
T'_{do}	time constant in exciter.
T_b	time constant in battery.
T_{HHO}	maximum iteration in HHO.
T_{INV}	time response of the BESS inverter.
T_{PV}	time constant of PVES.
T_S	temperature in STC.
T_W	wash-out filter constant.
U_B	upper bound.
X_{CO}	reactance in battery.
X_i	vector position of the hawk.
X_{rabbit}	vector position of the rabbit.
GCP	generation rate control parameter.
GP	generation probability.
H	inertia properties.
Y	rabbit's movement prediction by hawks.
Z	rabbit's pattern remap by hawks.
α_T	temperature coefficient of PV.
ΔE_{bt}	terminal equivalent in battery.
ΔE_{CO}	non-overlapping DC voltage.
ΔE_d	the relation between BESS and damping signal.
ΔP_{BESS}	change of generated electricity power from BESS.
ΔP_e	change of generated electricity power from conventional generators.
Δf	change of frequency or frequency deviation.
ΔGHI	change of solar GHI.
ΔP_{PV}	change of generated electricity power from PVES.
ΔP_L	change of load power demand.
ΔP_m	change of mechanical power.
ΔP_t	change of the total of generated electricity power.
ΔP_{VI}	change of VI power.
ΔP_{WT}	change of generated electricity power from WTES.
ΔW_{speed}	change of wind speed.
$\Delta\omega$	change of rotor speed.
$\Delta\delta$	change of power angle.
η	PV efficiency.
λ_A	eigenvalue of matrix A.
ξ_A	damping ratio.
ρ	air density.
σ_A	real part of eigenvalue representing damping factor properties.
Ω_A	imaginary part of eigenvalue representing oscillation properties.

LIST OF ABBREVIATIONS

AI	Artificial Intelligence.
AO	Arithmetic Optimizer.
ARSO	Adaptive Rat Swarm Optimizer.
AVR	Automatic Voltage Regulator.
BESS	Battery Energy Storage System.
CDI	Critical Damping Index.
ESS	Energy Storage System.
EO	Equilibrium Optimizer.
FLC	Fuzzy Logic Controller.
FPA	Flower Pollination Algorithm.
GA	Genetic Algorithm.
HHO	Harris Hawk Optimizer.
HHO-MSS	Harris Hawk Optimizer with Memory Saving Strategy.
IAE	Integral Absolute Error.
ISE	Integral Squared Error.
ITAE	Integral Time Absolute Error.
ITSE	Integral Time Squared Error.
LQR	Linear Quadratic Regulator.
LQG	Linear Quadratic Gaussian.
MOA	Mayfly Optimizer Algorithm.
PID	Proportional-Integral-Derivative.
POD	Power Oscillation Damper.
PSO	Particle Swarm Optimization.

PSS	Power System Stabilizer.
PV	Photovoltaic.
PVES	Photovoltaic Energy System.
QAGTO	Quantum Artificial Gorilla Troop Optimizer.
RoCoF	Rate of Change of Frequency.
RES	Renewable Energy Sources.
SCA-AOA	Sine Augmented Scaled Arithmetic Optimization Algorithm.
SMIB	Single Machine Infinite Bus.
SSSC	Static Synchronous Series Compensator.
STATCOM	Static Synchronous Compensator.
STC	Standard Test Condition.
SVC	Static Var Compensator.
VI	Virtual Inertia.
WT	Wind Turbine.
WTES	Wind Turbine Energy System.

I. INTRODUCTION

Renewable Energy Sources (RES) integration in power systems has become a trend. Photovoltaic Energy Systems (PVES) and Wind Turbine Energy Systems (WTES) are the two examples of most accessible RES with widespread utilization, ranging from small-scale installations (e.g. home, school, office, etc.) to large-scale installations (e.g. industrial, residential, remote islands, etc.) [1]. PVESs offer many benefits, such as producing no pollutants, requiring no fuel, and having low maintenance needs. Besides the PVES, the WTES can reduce carbon footprints and produce very low-cost electricity. Considering the benefits, the integration of PVES and WTES with conventional power systems through renewable microgrid power system technology is needed as a viable solution to maintain reliability, feasibility, and continuity in delivering power electricity worldwide [2], [3].

Besides the benefits, renewable microgrid power system poses a typical stability challenge. PVES and WTES are very dependent on uncertain natural conditions. These uncertainties result in fluctuations that can interfere stability of frequency, voltage, and power responses of the renewable microgrid power system [4]. The sudden changes in power input (both electrical power and mechanical power) and power load demands are considered minor disturbances. The minor disturbance that inflicts a small-signal oscillation must be mitigated properly before it goes to major disturbances and makes the system blackout. Therefore, the dynamic stability approach is conducted to analyze the minor disturbance in the power system [5].

Based on the dynamic stability approach, the damping and inertia concepts are very important in conventional generators to reduce the oscillation and return the system responses to its reference point when the disturbance occurs [6]. The additional controller, the Power System Stabilizer (PSS), is usually dispatched to add the damping properties [7]. The stability limits can be enhanced with PSS by regulating the excitation of the generator. Rotor speed or system frequency deviation signals are used as input for PSS to produce additional signals to the exciter. This signal triggers the exciter to produce electrical torque that can dampen the oscillations. The performance of PSS can be adjusted by controlling the tunable parameters. These tunable parameters delivers the lead/lag to compensate the amount of the different phases between rotor speed and electrical torque [8].

On the other hand, renewable microgrid power systems have different characteristics compared to conventional ones. Renewable microgrid power systems consist of inverter-based generators, with power electronic components, that do not possess damping and inertia properties [4]. This makes a renewable microgrid power system considered as an inertia-less system. Unfortunately, the general use of PSS is not effective in improving the stability of a renewable microgrid. Therefore, the Virtual Inertia (VI) concept is developed [9], [10]. Inertia properties can be imitated by using the VI concept. This inertia imitation can be emulated by controlling the behavior of the inverter and Energy Storage System (ESS). The VI emulation is related to rotor speed or frequency deviation, known as the Rate of Change of Frequency (RoCoF) of the system [4]. A renewable microgrid has a higher RoCoF resulting in a higher frequency nadir. This also makes the settling time longer. The VI emulation is dependent on the tunable parameters that can adjust the working behavior of the inverter and ESS. With this concept, VI emulation delivers a viable option to provide additional inertia properties in renewable microgrid power systems.

Along with the development of the modern power system, the renewable microgrid power system that consists of conventional and RES generators has wider working conditions. The wider working conditions result more complex stability improvement approach. The differences in RES penetration level need a specific approach to enhance the stability [11]. In low-RES penetration (0 to 25%), the conventional generator power is more dominant than the RES generator. In this condition, PSS is still reliable to enhance the stability. Otherwise, in high-RES penetration (75 to 100%), the VI controller is more effective in boosting stability when the RES generator output is more dominant. The more crucial problem appears when the power output from conventional and RES generators are similar (for example in 50% RES penetration). In this condition, stability controllers that can work in complement behavior in renewable microgrid power systems like PSS and VI are needed. In the current literature, the controlling parameters of PSS and VI are still limited. PSS has coordinated with the other stability controllers, e.g. Power Oscillation Damper (POD) [12], Static Synchronous Compensator (STATCOM) [13], Static Synchronous Series Compensator (SSSC) [14], Static Var Compensator (SVC) [15], etc. Those work results have significant stability improvements in various power system models. However, it is still limited to power systems with conventional generators. Thus, the controlling parameters of PSS and VI in renewable microgrid power systems need further investigation.

Controlling the parameters of PSS and VI needs the proper approach. This can be calculated manually with a mathematical approach. However, the approach has been developed to optimal and adaptive approaches, such as Linear Quadratic Regulator (LQR) and Linear Quadratic Gaussian (LQG) [16], [17], Proportional-Integral-Derivative (PID) [18], [19], etc. These approaches are very practical. However, the offered solution is sensitive to the initial point and requires a specific reference. In the modern era, the approach has rapidly evolved into Artificial Intelligence (AI)-based, such as intelligent algorithms. Fuzzy Logic Controller (FLC) is commonly used for controlling parameters in PSS or VI [20], [21]. FLC offers easy optimization rules. However, it does not give feedback if the rules are not suitable for the cases. Furthermore, the learning-based algorithm comes with the capability to learn and give feedback on whether the results are not going well. Reinforced and deep learning approaches have been implemented [22], [23]. For example, the Multi-Band Power System Stabilizer (MBPSS) is proposed with Deep Reinforcement Learning [24]. However, these approaches are very dependent on learning datasets. This is difficult to implement in unique cases with small datasets. Besides that, metaheuristic algorithms have been developed. Metaheuristic algorithms offer better exploration and exploitation mechanisms to find optimal results and are not dependent on rules or datasets [25], [26].

Genetic Algorithm (GA) and Particle Swarm Optimization (PSO) become the two most popular algorithms in controller parameter optimizations [7]. Nowadays, metaheuristic algorithms have rapidly developed with countless inspirations in the world and it has been implemented in modern power systems, including for controlling parameters in PSS or VI cases. For example, in [15] and [27], the Mayfly Optimizer Algorithm (MOA) has been applied for PSS-SVC and PSS-SSSC. Quantum Artificial Gorilla Troop Optimizer (QGTO), Harris Hawk Optimizer (HHO), Equilibrium Optimizer (EO), and Arithmetic Optimizer (AO) have been implemented in parameter tuning of PSS in Single Machine Infinite Bus (SMIB) and Multi Machine systems [8], [28], [29], [30]. Adaptive Rat Swarm Optimizer (ARSO) has been developed to find the optimal coordination of PSS and SVC [31]. In [32], Sine Augmented Scaled Arithmetic Optimization (SCA-AOA) has been used to find the optimal design of VI in regulating the frequency of a microgrid. In [33], the Flower Pollination Algorithm (FPA) has been combined with Fractional Order PID (FOPID) to solve frequency stabilization cases in a microgrid. Those studies concluded that a newer algorithm has better exploration and exploitation processes. However, sometimes a newer algorithm gets stuck or jumps to local optima, and is slower to converge because of complex operations.

From recent metaheuristic algorithms, HHO appeared as one of the popular algorithms due to its efficient solution tracking [34]. HHO adopts a brilliant mechanism of Harris Hawk in hunting their prey. HHO imitates the mechanism to conduct the dynamic patterns of exploration and exploitation processes [35]. HHO has been proven in large-scale research fields. For example: parameter identification for solar cell models [36], predicting the intention of students [37], image segmentation [38], drug design and discovery [39], speed and vehicle cruise control [40], [41], aircraft control system [42], etc. However, the solution tracking in HHO is sometimes stuck in local optima due to unbalanced exploration and exploitation proportions. Several modifications have been established. For example, the tent and chaotic map operators have helped HHO in increasing diversity to avoid being stuck in local optima [43]. Then, the Exploration Factor and Random Walk Strategy have been presented to improve the exploration and exploitation performance [44]. In [34] and [45], HHO has also been reported to be combined with the other algorithms to cover the drawbacks. However, HHO still leaves a challenge in the unbalanced proportion of exploration and exploitation.

Besides the mentioned shortcomings, metaheuristic algorithms need proper problem formulation to guarantee the result. In controlling parameters of PSS or VI cases, a basic objective function is usually formulated based on performance indexes. However, the accuracy is not ensured since the performance indexes only judge the dynamic stability performance from the output response. Thus, the objective function based on the eigenvalue component is established. Moreover, it can be found the combination of the objective function increases the accuracy. In [27], a combination of the damping ratio and frequency component is presented. The damping factor and damping ratio are also combined as the objective function [31]. Both [27] and [31] used the weighting sum scalarization technique. In this technique, determining these parameters is difficult and confusing due to each user having their preferences. Therefore, it needs an investigation for a better scalarization technique in controlling the parameters of PSS and VI.

Previous literature related to this work is summarized in Table 1. It can be seen the research gap between the existing work and the proposed work. It becomes motivation to solve the remaining challenge in the controlling parameter for PSS and VI, as in the following: 1) A proper approach is needed for controlling the parameters of PSS and VI to maximize the dynamic stability improvement in a renewable microgrid power system; 2) HHO as a recent novel metaheuristic algorithm is still leaving a challenge in the exploration and exploitation ability; 3) A better scalarization technique is needed for an innovative objective function in controlling the parameters of PSS and VI.

Based on the motivation to answer the mentioned challenges, this paper proposes a new approach based on a new scheme of HHO for controlling parameters of PSS and VI in the renewable microgrid power system. The significant contribution of this paper is detailed in the following:

1) This paper proposes a new approach for enhancing the dynamic stability of the renewable microgrid power

TABLE 1. Comparison between the previous works and the proposed work.

Previous works related to the controlling parameters for PSS or VI				
Ref.	**Controller**	**Optimizer**	**Objective Function**	**Notes**
[28]	Comparing conventional PSS, dual input PSS, TID-PSS	Quantum Artificial Gorilla Troops Optimizer (QAGTO)	Performance index based on ITSE	Implemented for Single Machine Infinite Bus (SMIB)
[8]	Conventional PSS	Hybrid Harris Hawk Optimizer – Equilibrium Optimizer Algorithm (HHHO-EOA)	Comparing IAE, ISE, ITAE, and ITSE as objective functions	Implemented for SMIB
[47]	Conventional PSS	Chaotic Version of HHO	Damping ratio	Implemented for IEEE 39-bus multimachine system
[15]	A hybrid of multi-band PSS2B and SVC	Mayfly Optimizer Algorithm (MOA)	Critical Damping Index (CDI)	Implemented for a real system in Indonesia (Sulselrabar Electricity System)
[31]	A hybrid of Conventional PSS and SVC	Adaptive Rat Swarm Optimizer (ARSO)	Combination of damping factor and damping ratio	Using weight-sum scalarization to combine the objective function
[27]	A hybrid of PSS and SSSC-POD	MOA	Combination of eigenvalue and frequency equations	Using weight-sum scalarization to combine the objective function
[48]	VI	Particle Swarm Optimization (PSO)	ITAE	Implemented for two-area interconnected power system with a PV system
[49]	VI	Firefly Algorithm (FA)	ITAE	Implemented for two-area interconnected power system with a PV system
[32]	VI	Sine Augmented Scaled Arithmetic Optimization Algorithm (SCA-AOA)	ISE	Implemented for a microgrid with renewables
[33]	FOPID-VI	Flower Pollination Algorithm (FPA)	Change of frequency equation	Implemented for a microgrid with renewables
Proposed Work	**A hybrid of dual input PSS and VI**	**A new scheme of Harris Hawk Optimizer with Memory Saving Strategy (HHO-MSS)**	**Combination of damping factor and damping ratio**	**Implemented for a microgrid with a conventional generator, PVES, WTES, and BESS. Using Benson Scalarization to combine the objective function**

Previous works related to the HHO modification			
Ref.	**Modification**	**Implementation**	**Notes**
[8]	Hybrid Harris Hawk Optimizer – Equilibrium Optimizer Algorithm (HHHO-EOA)	Optimal tuning for PSS	The modification aims to enhance the exploration and exploitation ability in general.
[47]	Chaotic version of HHO	Optimal tuning for PSS	The modification aims to improve static operators and enhance global searching.
[43]	Chaotic version of HHO	Engineering benchmark function	The modification aims to repair the random variables in exploration and exploitation procedures to avoid the local optima.
[44]	Adding the exploration factor and random walk strategy operators for HHO	Various benchmark and CEC2017 functions	The modification aims to improve the ability in the exploration and exploitation process and help the algorithm to jump out from local optima.
Proposed Work	**A new scheme of Harris Hawk Optimizer with Memory Saving Strategy (HHO-MSS)**	**Controlling Parameters for PSS and VI in the renewable microgrid power system**	**The modification aims to balance exploration and exploitation proportions to enhance the ability and ensure the quality of global optima.**

system by performing the hybrid controlling parameters of PSS and VI. The investigated system consists of conventional generators, PVES, WTES, and Battery Energy Storage System (BESS).

2) A new scheme of Harris Hawk Optimizer with Memory Saving Strategy (HHO-MSS) is proposed as a robust optimizer. The modification is inspired by EO operators [46] and is expected to escalate the exploration and exploitation ability and ensure the optimal solution.
3) Benson Scalarization Technique is introduced for controlling parameters for PSS and VI to provide innovative objective functions dependent on a combination of the damping factor and damping ratio.

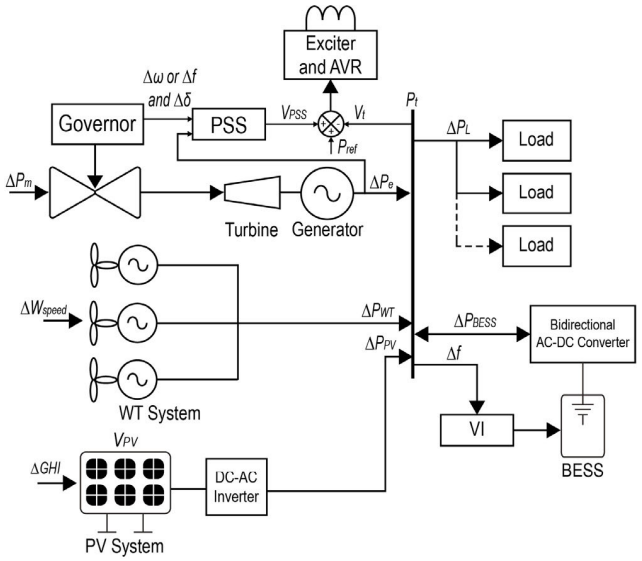

FIGURE 1. The renewable microgrid and controller models.

The organization of this paper is described as follows: Section II illustrates the renewable microgrid power system with PSS and VI models. Section III describes the proposed new approach for controlling the parameters of PSS and VI based on the HHO-MSS and Benson Scalarization Technique. Section IV delivers the proposed algorithm performance benchmarking using the Friedman Ranking Test, convergence curve, and proportion analysis. The optimal parameters of PSS and VI results are investigated by eigenvalue and time domain analysis. Furthermore, the validation with performance indexes is also given. In the rest, Section V highlights the result of the contribution.

II. POWER SYSTEM AND CONTROLLER DESIGNS

In this section, the renewable microgrid power system with PSS and VI models is illustrated. The simplified dynamic model for the power systems is established. Most dynamic stability studies used the simplified model due to easiness and clearness in the analysis [50], [51], [52]. The complex modeling can distract the focus of the dynamic behavior of the power systems. This model consists of power generation with a conventional generator that is connected to PSS, and RES generators including PVES and WTES. Besides that, BESS is also conducted to realize the VI emulation. The illustration of the renewable microgrid power system in this paper is given in Figure 1.

A. POWER GENERATION DESIGN

The power generation mathematic model is conducted based on the change of the total of generated electricity power (ΔP_t). from conventional generators (ΔP_e), WTES (ΔP_{WT}), PVES (ΔP_{PV}), and BESS (ΔP_{BESS}). To maintain the stability of the power system, ΔP_tmust be equal to load power demand (ΔP_L). The relation between $\Delta P_t$and ΔP_L is given by Equation (1) and Equation (2).

$$\Delta P_t = \Delta P_L \tag{1}$$

$$\Delta P_e + \Delta P_{WT} + \Delta P_{PV} \pm \Delta P_{BESS} = \Delta P_L \tag{2}$$

In dynamic stability, the change of mechanical power (ΔP_m) of generators must be equal to ΔP_e as in Equation (3). Besides, the ΔP_m is related to the inertia (H), damping (D), and frequency deviation (Δf) properties as in Equation (4).

$$\Delta P_m = \Delta P_e \tag{3}$$

$$\Delta P_m = 2Hs\,(\Delta f) + D(\Delta f) \tag{4}$$

with:

1) If $P_m > P_e$, then $\Delta f > 0$. $\Delta\omega$ and Δf are increased.
2) If $P_m < P_e$, then $\Delta f < 0$. $\Delta\omega$ and Δf are decreased.
3) If $P_m = P_e$, then $\Delta f = 0$. $\Delta\omega$ and Δf are constant.

To reach decent dynamic stability in the power system, the Δf must be maintained properly. Therefore, the dynamic stability equation represented by Δf can be obtained by substituting Equation (2) to Equation (4) as in Equation (5).

$$\Delta f = \frac{1}{2Hs + D}(\Delta P_m + \Delta P_{WT} + \Delta P_{PV} \pm \Delta P_{BESS} - \Delta P_L) \tag{5}$$

1) CONVENTIONAL GENERATOR MODEL

In this paper, an area power system with a certain group of generators is demonstrated. This system consists of a synchronous generator, turbine, governor, exciter, and Automatic Voltage Regulator (AVR). In the dynamic stability study, the torque change caused by the governor is ignored. It drives the exciter to be responsible for mitigating the small disturbances within 0.1 to 2 Hertz (Hz). This condition makes the exciter become less able to tackle that situation. Therefore, a PSS as the additional controller is dispatched to respond the small disturbances. The 4$^{\text{th}}$-order equation is used to model the dynamic behavior of the power system as given in Equation (6) until Equation (10) [28].

$$\dot{\delta} = \omega_r(\omega - 1) \tag{6}$$

$$\dot{\omega} = \frac{(P_M - P_E - D_\omega)}{M} \tag{7}$$

$$\dot{E}'_q = \frac{[-E'_q + E_{fd} - (x_d - x'_d)\, i_d]}{T'_{do}} \tag{8}$$

$$\dot{E}'_{fd} = \frac{[k_A\,(V_{ref} - V_t - V_{PSS}) - E_{fd}]}{T_E} \tag{9}$$

$$P_e = E'_q i_q + (x_d - x'_d)\, i_d i_q \tag{10}$$

To make the dynamic modeling easier, these equations can be employed in the simplified model from the Heffron-Phillips as given in Equation (11) until Equation (14).

$$\dot{\Delta\delta} = \omega_r \Delta\omega \tag{11}$$

$$\dot{\Delta\omega} = -\frac{K_1}{2H}\Delta\delta - \frac{D}{2H}\Delta\omega - \frac{K_2}{2H}E'_q \tag{12}$$

$$\Delta\dot{E}'_q = \frac{K_4}{T'_{do}}\Delta\delta - \frac{\Delta E'_q}{T'_{do}K_3} + \frac{E_{fd}}{T'_{do}} \quad (13)$$

$$\Delta\dot{E}'_{fd} = -\frac{k_A K_5}{T_A}\Delta\delta - \frac{k_A K_6}{T_A}\Delta E'_q - \frac{E_{fd}}{T_A} + \frac{k_A}{T_A}\Delta V_{PSS} \quad (14)$$

with $\Delta\delta$ is change of power changes, ω_r is rotor's synchronous speed, $\Delta\omega$ is rotor speed changes or frequency deviation, E'_q is terminal voltage, T'_{do} is the time constant in exciter, E_{fd} is the exciter's output voltage, k_A is the amplifier's gain constant in the exciter, T_A is the amplifier's time response constant. K_1 until K_6 represents the dynamic behavior based on the Heffron-Phillips model.

2) PVES MODEL

In general, the PVES can be modeled based on the PV output characteristics as given in Equation (15) [2].

$$\Delta P_{PV} = \eta \times N_{PV} \times \left(\frac{R}{R_S}\right) \times [1 + \alpha_T(T - T_S)] \quad (15)$$

with η is PV efficiency, N_{PV} is the power-rated of PV, R is solar GHI, R_S is solar GHI in Standard Test Condition (STC) = 1 kW/m^2, α_T is the temperature coefficient of PV, T is ambient temperature, and T_S is the temperature in STC = 25 ^{o} C. T is assumed to be 25 ^{o}C.

In the dynamic stability study, the simplified PVES model based on low order equation is adequate to investigate the dynamic behavior in the renewable microgrid power system [4], [9], [53]. Therefore, it can be obtained the dynamic model of the PVES as shown in Equation (16) with ΔP_{PV} is only linearly affected by ΔGHI.

$$G_{PV}(s) = \frac{K_{PV}}{1 + sT_{PV}} = \frac{\Delta P_{PV}}{\Delta GHI} \quad (16)$$

with K_{PV} and T_{PV} are the gain and time response constants of the PVES.

3) WTES MODEL

In common, the WTES model can be defined based on the WTES output characteristics as given in Equation (17) [54].

$$\Delta P_{WT} = \frac{1}{2}\rho A C_p W^3_{speed} \quad (17)$$

with ρ is air density constant = 1.25 kg/m^3, A is the swept area by the wind turbine, C_P is the power coefficient of WT, and W_{speed} is the wind speed variable.

Similar to the PVES model, the simplified WTES model based on low order equation is also adequate to represent the dynamic behavior. Thus, the WTES can be defined as in Equation (18).

$$G_{WT}(s) = \frac{K_{WT}}{1 + sT_{WT}} = \frac{\Delta P_{WT}}{\Delta W_{speed}} \quad (18)$$

4) BESS MODEL

The simplified dynamic model of BESS is conducted as in Figure 2. This model is specifically modeled to accommodate the BESS behavior in frequency regulation [49], [55]. This model has focused on active power injection in a short time.

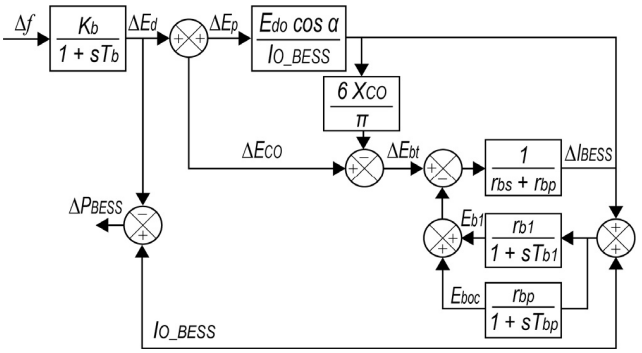

FIGURE 2. Dynamic model of BESS.

The relation of BESS and frequency regulation with the damping signal (ΔE_d) approach is given in Equation (19).

$$\Delta E_d = \frac{K_b}{1 + sT_b}\Delta f \quad (19)$$

with K_b is the control gain constant and T_b is the time response constant in a battery. I_{O_BESS} is DC through BESS, ΔE_{CO} is non-overlapping DC voltage, X_{CO} is reactance, ΔE_{bt} is terminal equivalent, E_{b1} is maximum overvoltage, E_{boc} is open circuit voltage, r_{bs} is internal resistance, r_{bp} is self-discharge resistance, and r_{b1} is overvoltage resistance.

B. PSS DESIGN

The concept of dynamic stability improvement by PSS is shown in Equation (9). The PSS can inject the additional signal (V_{PSS}) to the exciter to adjust the magnetic flux that is related to electrical torque. The PSS usually used the $\Delta\delta$, $\Delta\omega$, or Δf as the reference for the current condition of stability. V_{PSS} can be obtained by Equation (20).

$$V_{PSS} = K_{PSS}\left[\frac{sT_w}{1 + sT_w}\right]\left[\frac{(1 + T_1 s)}{(1 + T_2 s)}\frac{(1 + T_3 s)}{(1 + T_4 s)}\right]\Delta f \quad (20)$$

with K_{PSS} is a gain constant of PSS, T_W is a wash-out filter constant, and T_1, T_2, T_3, and T_4 are the tunable parameters of PSS. The tunable parameters provide additional signals that compensate for lead or lag in the output response in the $\Delta\delta$, $\Delta\omega$, or Δf of the power system.

In this paper, the dual-input PSS is dispatched to conduct better performance [56]. The dynamic model of dual-input PSS is shown in Figure 3. This model has three gain constants (K_{PSS}, K_{PSS2}, and K_{PSS3}), four wash-out filters (T_{W1}, T_{W2}, T_{W3}, and T_{W4}) followed by lag control time constants (T_6, and T_7). This model also established the ramp-tracking features represented by M and N with T_8 and T_9.

C. VI DESIGN

The dynamic model of VI is primarily focused on the dynamic behavior of frequency regulation [4]. The input of VI is $\Delta\omega$ or Δf. The VI emulation can be conducted by combining the first order model of BESS inverter and VI

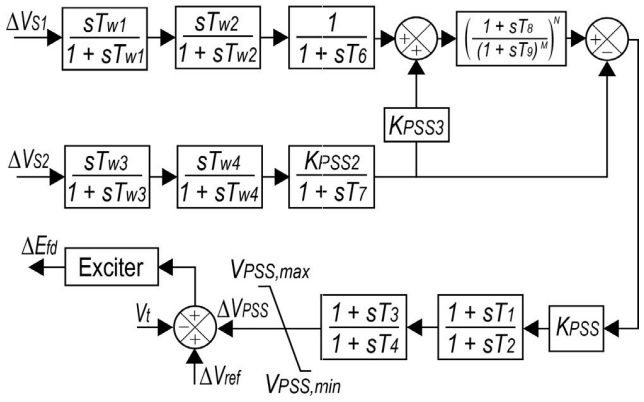

FIGURE 3. Dynamic model of dual-input PSS.

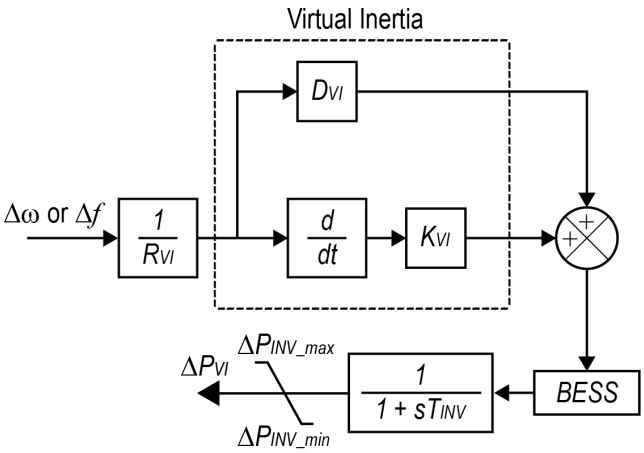

FIGURE 4. The dynamic model of the VI.

droop model as illustrated in Figure 4. The dynamic equation of VI power (ΔP_{VI}) is given in Equation (21).

$$\Delta P_{VI}(s) = \frac{sK_{VI} + D_{VI}}{1 + sT_{INV}} \left(\frac{\Delta f(s)}{R_{VI}} \right) \tag{21}$$

with R_{VI} is the VI droop constant, D_{VI} is the virtual damping constant generated by VI, K_{VI} is the VI gain constant, and T_{INV} is the time response of the BESS inverter.

Based on Figure 4 and Equation (21), the VI emulation is conducted by a derivative approach to calculate the RoCoF (df/dt). This model uses RoCoF as a reference for injecting P_{VI} to decrease the oscillation in $\Delta\omega$ or Δf. Besides, the virtual damping can imitate the damper effect like in the mechanical part of the generator. The filter and limiter (P_{INV_max} and P_{INV_min}) are regulated by the BESS inverter. This filter and limiter are useful for wiping out the noise and performing a proper dynamic behavior with a fast response. Thus, the description can explain the VI mechanism in imitating the properties of the conventional generator to the renewable microgrid power system.

III. PROPOSED APPROACH IN CONTROLLING PARAMETERS OF PSS AND VI

In this section, the proposed approach for controlling the parameters of PSS and VI based on the HHO-MSS and Benson Scalarization Technique is presented. A problem formulation is described. Besides that, the proposed scheme of HHO-MSS is illustrated in a detailed flowchart and comprehensive explanation.

A. PROBLEM FORMULATION

The problem formulation is focused on indicating the stability performance of the renewable microgrid power system. This paper has used the stability assessment based on the eigenvalue components. Thus, it is needed to convert the mathematical model into the state-space model. The linear state-space representation is given in Equation (22) and Equation (23).

$$\dot{x}(t) = Ax(t) + Bu(t) \tag{22}$$

$$y(t) = Cx(t) + Du(t) \tag{23}$$

with A is the $n \times n$ matrix that represents the renewable microgrid power system conditions, B is the $n \times p$ matrix of inputs, C is $q \times n$ matrix of outputs, and D is $q \times p$ matrix of transition. Then, $x(t)$ represents the renewable microgrid power system variables as given in Equation (24), $u(t)$ represents input variables as given in Equation (25), and $y =$ output as in Equation (26).

$$x(t) = [\Delta f\, \Delta\delta\, \Delta P_m\, \Delta P_{WT}\, \Delta P_{PV}\, \Delta P_{BESS}\, \Delta P_{VI}\, \Delta V_{PSS}] \tag{24}$$

$$u(t) = [\Delta GHI\, \Delta W_{speed}\, \Delta P_L] \tag{25}$$

$$y = [\Delta f\, \Delta\delta] \tag{26}$$

Thus, the eigenvalue can be obtained by extracting the determinant of matrix A by Equation (27).

$$det(sI - A) = 0 \tag{27}$$

with I is the identity matrix and s is the eigenvalue of A. The eigenvalue is obtained as $n \times n$ dimension of matrix A. The eigenvalue of matrix A (λ_A) is given as in Equation (28).

$$\lambda_A = \sigma_A + \Omega_A \tag{28}$$

with σ_A is a real part that represents the damping factor properties and Ω_A is an imaginary part that represents oscillation properties.

Besides that, it can also be obtained damping ratio (ξ_A) from matrix A by Equation (29).

$$\xi_A = \frac{-\sigma_A}{\sqrt{\sigma_A^2 + \Omega_A^2}} \tag{29}$$

This paper has used two objective functions based on damping factor and damping ratio properties as given in Equation (30) and Equation (31).

$$f_1 = \sum_{\sigma_i \geq \sigma_0} (\sigma_0 - \sigma_1) \tag{30}$$

TABLE 2. Typical range for PSS and VI parameters.

Parameter	Lower Bound (L_B)	Upper Bound (U_B)
K_{PSS}	0.01	10
T_1	0.01	0.2
T_2	0.01	0.2
T_3	0.01	0.2
T_4	0.01	0.2
K_{VI}	0.1	10
D_{VI}	0.1	2

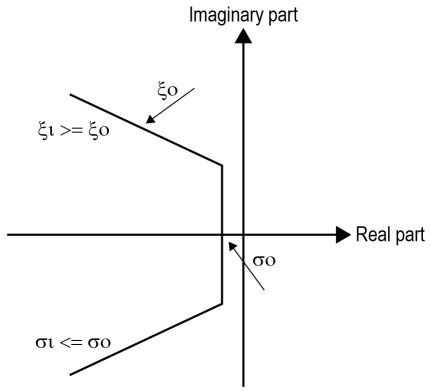

FIGURE 5. D-shape region of stability.

$$f_2 = \sum_{\xi_i \geq \xi_0} (\xi_0 - \xi_1) \tag{31}$$

with σ_0 and ξ_0 are the initial value of the system conditions, while σ_1 and ξ_1 are the values when the control variables are injected.

The fitness value calculation from the objective function differs based on control variables. The control variables are the tunable parameters in PSS and VI. As in Figure 3, the tunable parameters in the PSS are K_{PSS}, T_1, T_2, T_3, and T_4. Meanwhile in VI, as given in Figure 4, the tunable parameters are K_{VI} and D_{VI}. These variables need to be controlled optimally. Thus, Equation (30) and Equation (31) can be written as Equation (32) and Equation (33).

$$f_1 = \sum_{\sigma_i \geq \sigma_0} (\sigma_0 - \sigma_1(K_{PSS}, T_1, T_2, T_3, T_4, K_{VI}, D_{VI})) \tag{32}$$

$$f_2 = \sum_{\xi_i \geq \xi_0} (\xi_0 - \xi_1(K_{PSS}, T_1, T_2, T_3, T_4, K_{VI}, D_{VI})) \tag{33}$$

The typical range for PSS and VI parameters is shown in Table 2. The search space is determined based on technical recommendations for PSS and VI implementation in a single-area power system [4], [50], [56]. Then, the limit of stability is validated with the D-shape region of stability properties as given in Figure 5. Thus, the D-shape is considered as problem constraints.

B. INNOVATIVE OBJECTIVE FUNCTION DEPENDENT ON BENSON SCALARIZATION TECHNIQUE

The Benson Scalarization Technique is used to combine Equation (32) and Equation (33). This technique does not need any parameter from the user, such as objective weight and reference point like in the other scalarization techniques [57], [58]. This scalarization technique serves a set of initial proper solutions stated in $f_1(x^o)$ and $f_2(x^o)$. To find the best solution or the best fitness value of the functions $f_1(x)$ and $f_2(x)$, the difference value of these two functions must be maximized. The general equation of the Benson Scalarization Technique is represented by the positive difference of the first and second functions (l_1 and l_2) as shown in Equation (34).

$$f_{benson's}(x) = \max(l_1 + l_2) \tag{34}$$

with l_1 and l_2 calculate the difference between an initial fitness value ($f_1(x^o)$) and the fitness values on iterations $f_1(x)$ as shown in Equation (35).

$$f_{benson's}(x) = \max[\left(f_1\left(x^o\right) - f_1(x)\right) + \left(f_2\left(x^o\right) - f_2(x)\right)] \tag{35}$$

By constituting Equation (32) and Equation (33) into Equation (35), it can be obtained the proposed objective function as shown in Equation (36).

$$\begin{aligned} &f_{benson's}(x) \\ &= \max\left[\left(\sum\nolimits_{\sigma_i \geq \sigma_0} (\sigma_0 - \sigma_1(CV))^O - \sum\nolimits_{\sigma_i \geq \sigma_0} (\sigma_0 - \sigma_1(CV))\right)\right. \\ &\quad \left. + \left(\sum\nolimits_{\xi_i \geq \xi_0} ((\xi_0 - \xi_1(CV))^O - \sum\nolimits_{\xi_i \geq \xi_0} (\xi_0 - \xi_1(CV))\right)\right] \end{aligned} \tag{36}$$

with CV is control variables: $K_{PSS}, T_1, T_2, T_3, T_4, K_{VI}, D_{VI}$.

C. HHO OVERVIEW

HHO is the recent and robust metaheuristic optimizer that is classified as a nature-inspired algorithm [35], [45]. HHO imitates the unique hunting strategy of a flock of Harris Hawk. A flock of Harris Hawks can communicate and coordinate with the group hunting members in searching, trailing, besieging, and catching their prey, which is usually a rabbit. In this paper, HHO is explained in the following phases: pre-hunting, exploration, transition, exploitation, and post-hunting.

1) PRE-HUNTING PHASE

Harris Hawks are initiated to make a group before begin to hunt. This group members usually consists of their family or flock. The members of hunting groups are usually spread away to look for their potential prey. In HHO, this phase begins with defining the number of populations (N_{HHO} and the maximum iteration (T_{HHO}). A random population of the hawks is initiated with their respective positions (X_i, $i = 1, 2, \ldots, N_{HHO}$). The hawk represents the candidate's solutions. Then, HHO evaluates the fitness value of each X_i with a

predetermined objective function. In the next step, the position of the rabbit (X_{rabbit}) is determined randomly based on the search space. The rabbit represents the best candidate's solution. The rabbit has an initial energy parameter (E_o) and jump strength (J). The E_o value is defined as the fitness value of X_{rabbit}. Besides, the escaping energy of the rabbit (E) is determined and updated along the iteration (t_{HHO}) as given in Equation (37).

$$E = 2E_0(1 - \frac{t_{HHO}}{T_{HHO}}) \tag{37}$$

2) EXPLORATION PHASE

This phase illustrates the hawks perching randomly in the branches. They observe and communicate with each other to decide the potential rabbit to hunt. Then, the hawks move regularly to perch on tall trees. This perching position is determined based on the q, which has a random value between 0 to 1. If $q \geq 0.5$, then the hawk perches randomly. While $q < 0.5$, the hawk perches near the rabbit and considers the average distance in the hunting group. The position of the hawk is updated by Equation (38) and the average position of the hunting group is calculated by Equation (39).

$$X\,(t_{HHO}+1) = \begin{cases} X_{rand}\,(t_{HHO}) - r_1|X_{rand}(t_{HHO}) \\ -2r_2X(t_{HHO})|, & q \geq 0.5 \\ X_{rabbit}(t_{HHO}) - X_m(t_{HHO}) \\ -r_3(L_B + r_4(U_B - L_B)), & q < 0.5 \end{cases} \tag{38}$$

$$X_m\,(t_{HHO}) = \frac{1}{N_{HHO}} \sum_{i=1}^{N_{HHO}} X_i(t_{HHO}) \tag{39}$$

with $X_{rand}(t_{HHO})$ is a random movement of the hawk in iteration related to the current hawk's position ($X(t_{HHO})$). $X_{rabbit}\,(t_{HHO})$ represents the location of the rabbit. The r_1–r_4 are random values between 0 to 1 to impersonate the randomness of animal behavior in nature.

3) TRANSITION PHASE

The hunting group of the hawks observes and estimates the rabbit condition. In HHO, this behavior belongs to the transition phase. The transition in HHO is influenced by E_o and E as shown in Equation (40) and Equation (41).

$$E_o = \begin{cases} E_o, 0 \gg 1, & \textit{the rabbit has a lot of energy} \\ E_o, 1 \gg 0, & \textit{the rabbit is run out of energy} \end{cases} \tag{40}$$

$$phase(E) = \begin{cases} |E| \geq 1, & phase \gg exploration \\ |E| < 1, & phase \gg exploitation \end{cases} \tag{41}$$

In Equation (40), the increase in E_o from 0 to 1 represents that the rabbit still has a lot of energy and confidence. Whereas the decrease in E_o from 1 to 0 represents the rabbit is running out of energy and exhausted. If $|E| \geq 1$, then the hawks are still in the exploration phase. While $|E| < 1$, then the hawks advance to the exploitation phase.

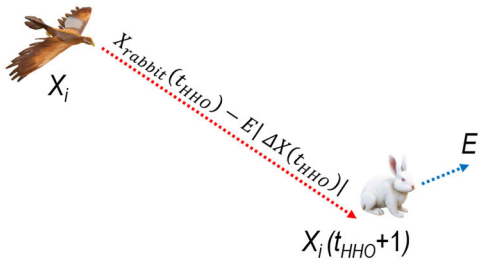

FIGURE 6. Hard besiege illustration in HHO.

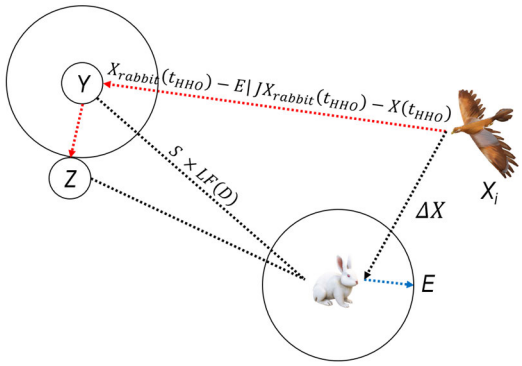

FIGURE 7. Soft besiege with progressive rapid dives illustration in HHO.

4) EXPLOITATION PHASE

HHO has adopted a dynamic hunting mechanism based on different rabbit conditions [35]. In HHO, the hunting mechanism is performed depending on two parameters, $|E|$ and the rabbit's escape probability (r). The r is a random value between 0 and 1. If $r < 0.5$, then the rabbit has a big chance of escaping. If $r \geq 0.5$, then the rabbit has a small chance of escaping. HHO impersonates the hunting in four mechanisms as follows:

a: SOFT BESIEGE

A hunting group of hawks performs the soft besiege mechanism when the rabbit still has a lot of energy. It indicates the rabbit is trying to escape. The hawks surround the rabbit and take turns attacking the rabbit with soft besiege to weaken the rabbit before launching the surprise attacks. The soft besiege is shown in Equation (42) and Equation (43) with J calculated by Equation (44).

$$X\,(t_{HHO}+1) = \Delta X\,(t_{HHO}) - E|JX_{rabbit}\,(t_{HHO}) - X\,(t_{HHO})\,| \tag{42}$$

$$\Delta X(t_{HHO}) = X_{rabbit}\,(t_{HHO}) - X(t_{HHO}) \tag{43}$$

$$J = 2(1 - r_5) \tag{44}$$

with $\Delta X_{(t_{HHO})}$ represents the distance between the hawks and the rabbit. The r_5 is a random value between 0 to 1.

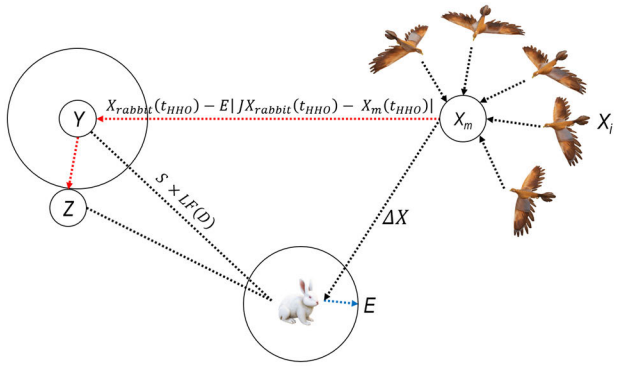

FIGURE 8. Hard besiege with progressive rapid dives illustration in HHO.

b: HARD BESIEGE

A hunting group of hawks performs the hard besiege mechanism when the rabbit is starting to get tired. The hawks surround the rabbit, perform heavy attacks, and launch a surprise attack to quickly end the hunt. The hard besiege is illustrated in Equation (45) and Figure 6.

$$X(t_{HHO}+1) = X_{rabbit}(t_{HHO}) - E|\Delta X(t_{HHO})| \tag{45}$$

c: SOFT BESIEGE WITH PROGRESSIVE RAPID DIVES

This condition represents the rabbit which still has a lot of energy after successfully escaping. The rabbit performed random frog jumps, the Levy Flight (LF) movement. In this condition, the hawks estimate the pattern of the rabbit movement (Y) based on Equation (46). If the hawks fail to catch the rabbit, then the hawks perform random dives to remap the rabbit pattern (Z) as in Equation (47). The LF is modeled as in Equation (48). The attack pattern is updated dependent on Equation (49). The soft besiege with progressive rapid dives mechanism is given in Figure 7.

$$Y = X_{rabbit}(t_{HHO}) - E|JX_{rabbit}(t_{HHO}) - X(t_{HHO})| \tag{46}$$

$$Z = Y + S \times LF(D) \tag{47}$$

$$LF(x) = 0.01 \times \left(\frac{\mathfrak{u} \times \sigma}{|v|^{\frac{1}{\beta}}}\right).$$

$$\sigma = \left(\frac{\Gamma(1+\beta) \times \sin(\frac{\pi\beta}{2})}{\Gamma\left(\frac{1+\beta}{2}\right) \times \beta \times 2^{\frac{\beta-1}{2}}}\right) \tag{48}$$

$$X(t_{HHO}+1) = \begin{cases} Y \text{ if } F(Y) < F(X(t_{HHO})) \\ Z \text{ if } F(Z) < F(X(t_{HHO})) \end{cases} \tag{49}$$

with D is the problem dimension and S is a random vector by size $1 \times D$. $\mathfrak{u}$ and v are the random values between 0 to 1. β is the constant that is set to be 1.5.

d: HARD BESIEGE WITH PROGRESSIVE RAPID DIVES

This condition represents the rabbit which no longer has enough energy after trying to escape from the surprise attack.

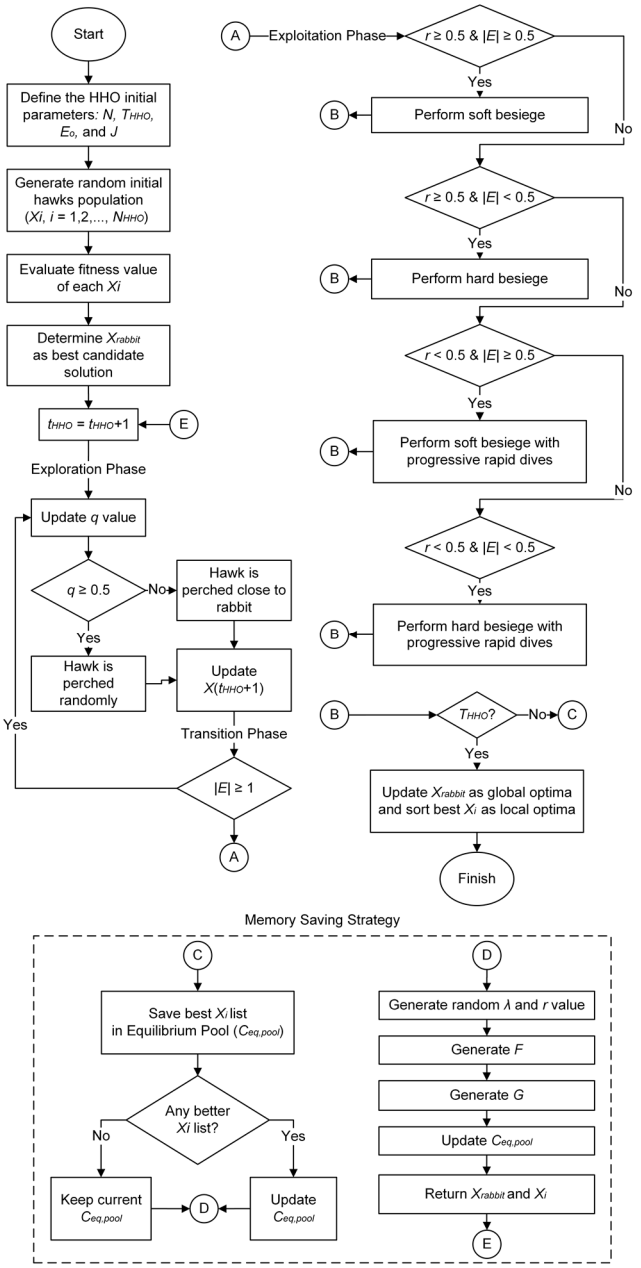

FIGURE 9. A new scheme of Harris Hawk Optimizer with Memory Saving Strategy (HHO-MSS).

The hunting mechanism of the hawks is similar to the soft besiege. However, the hawks reduce their average distance from the rabbit before launching a surprise pounce. The hawks decide on attack patterns by Equation (49). However, the Y and Z rules have changed into Equation (50) and Equation (51). The hard besiege with progressive rapid dives mechanism is illustrated in Figure 8.

$$Y = X_{rabbit}(t_{HHO}) - E|JX_{rabbit}(t_{HHO}) - X_m(t_{HHO})| \tag{50}$$

$$Z = Y + S \times LF(D) \tag{51}$$

TABLE 3. Benchmarking scenarios of the algorithms.

Algorithm	Note	Parameter	Value
#1 HHO-MSS	The proposed algorithm in this paper.	N_{HHO}	30
		T_{HHO}	100
		D	30
		q	rand(0,1)
		E_o	rand(-1,1)
		u, v, λ	rand(0,1)
		β	1.5
		a_1	2
		a_2	1
		GCP	0.5
		$r_1 - r_8$	rand(0,1)
#2 Iteration-based of Hybrid HHO-EO [8]	The hybridization of algorithms by running the optimization process sequentially.	N	30
		T_{HHO}	50
		T_{EO}	50
#3 Population-based of Hybrid HHO-EO [8]	The hybridization of algorithms by running two algorithms in parallel and sharing their best solution.	N_{HHO}	15
		N_{EO}	15
		T	100
#4 Basic HHO [35]	The original version of HHO.	N_{HHO}	30
		T_{HHO}	100
		D	30
		q	rand(0,1)
		E_o	rand(-1,1)
		u, v	rand(0,1)
		β	1.5
		$r_1 - r_5$	rand(0,1)
#5 Basic EO [46]	The original version of EO	N_{EO}	30
		T_{EO}	100
		D	30
		λ	rand(0,1)
		a_1	2
		a_2	1
		GCP	0.5
		r,r_1, r_2	rand(0,1)

5) POST-HUNTING PHASE

At the end of the hunting process, the hawks usually distribute the hunting results to the hunting group's members who participate in the hunt. In HHO, the end of the hunting process is shown by the E value near zero. In HHO, X_{rabbit} in the last iteration is defined as the best solution.

D. PROPOSED HHO-MSS

The HHO-MSS enhances the HHO with a memory saving operator inspired by an Equilibrium Optimizer (EO). EO is one of the metaheuristic optimizers that is classified as a physic-based inspiration algorithm [46]. EO adopts the concept of controlling volume mass balance in a substance. EO has an operator to control the balance of exploration and exploitation. The proposed modification is unlike the common hybrid algorithm that runs two algorithms in parallel or only divides the population or iteration sequentially. The detailed flowchart of HHO-MSS is given in Figure 9. A comprehensive description is also given in the following:

First, HHO-MSS performs the usual mechanism in HHO, including pre-hunting, exploration, transition, exploitation, and post-hunting phases. The idea is to sort the hawks with the best movement that gives the closest distance to the rabbit. The proposed scheme adopts the equilibrium pool ($C_{eq,pool}$) in EO. $C_{eq,pool}$ is used to keep the best hawk positions, $X_i,\ldots,$ X_N, as the current candidate solutions as in Equation (52).

$$C_{eq,pool} = [X_1, X_2, X_3, \ldots, X_N] \tag{52}$$

$$C_{eq,pool} = \begin{cases} if\ X_{rabbit,t_{HHO}} \geq X_{rabbit,t_{HHO}+1}, \\ X_{rabbit,t_{HHO}} = X_{rabbit,t_{HHO}} \\ if\ X_{i,t_{HHO}} \geq X_{i,t_{HHO}+1}, \\ X_{i,t_{HHO}} = X_{i,t_{HHO}} \end{cases} \tag{53}$$

$$C_{eq,pool} = \begin{cases} if\ X_{rabbit,t_{HHO}} < X_{rabbit,t_{HHO}+1}, \\ X_{rabbit,t_{HHO}} = X_{rabbit,t_{HHO}+1} \\ if\ X_{i,t_{HHO}} < X_{i,t_{HHO}+1}, \\ X_{i,t_{HHO}} = X_{i,t_{HHO}+1} \end{cases} \tag{54}$$

$C_{eq,pool}$ components are updated regularly based on Equation (53) and Equation (54). If Xi in the current iteration is better than on the next iteration, then keep the components of $C_{eq,pool}$. Meanwhile, Xi on the next iteration is better than in the current iteration, then replaces the components of $C_{eq,pool}$.

The proposed scheme has also adopted the exponential factor (F) and generation rate (G) operators from EO. These operators are related to the controllability of the exploration and exploitation proportion. The F operator is described in Equation (55) until Equation (57).

$$F = e^{\lambda(t_{HHO} - t^{O}_{HHO})} \tag{55}$$

$$t_{HHO} = (1 - \frac{t_{HHO}}{T_{HHO}})^{(a_2 \frac{t_{HHO}}{T_{HHO}})} \tag{56}$$

$$t^{O}_{HHO} = \frac{1}{\lambda}\ln(-a_1 sign\,(r_6 - 0.5)\left[1 - e^{-\lambda t_{HHO}}\right] + t_{HHO}) \tag{57}$$

with t_{HHO} is the function of iteration, it decreases with the number of iterations, while t^{O}_{HHO} is variable to make the search speed slow down to ensure convergence. The λ and r_6 related to the direction of candidate solutions movement, which is the values between 0 to 1. The a_1 is the control parameters of exploration and a_2 is the control parameter of exploitation. Based on [46], the best balance can be obtained with $a_1 = 2$ and $a_2 = 1$.

The G operator is shown in Equation (58) until Equation (60). This parameter is used to control the search pattern and limit the number of randomness of candidate solutions.

$$G = G_o e^{-\lambda(t_{HHO} - t^{O}_{HHO})} \tag{58}$$

$$G_o = GCP(C_{eq} - \lambda C_{eq,pool}) \tag{59}$$

TABLE 4. Unimodal benchmark functions for HHO-MSS benchmarking.

	No	Function	Search Space	*D*	f_{min}
Unimodal benchmark functions	f_1	$f_1(x) = \sum_{i=1}^{D} x_i^2$	(-100, 100)	30	0
	f_2	$f_2(x) = \sum_{i=1}^{D} \lvert x_i \rvert + \prod_{i=1}^{D} \lvert x_i \rvert$	(-10, 10)	30	0
	f_3	$f_3(x) = \sum_{i=1}^{D} \left(\sum_{j=1}^{D} x_j \right)^2$	(-100, 100)	30	0
	f_4	$f_4(x) = max_i\{\lvert x_i \rvert, 1 \le i \le D\}$	(-100, 100)	30	0
	f_5	$f_5(x) = \sum_{i=1}^{D-1} [100(x_{i+1} - x_i^2)^2 + (x_i - 1)^2]$	(-30, 30)	30	0
	f_6	$f_6(x) = \sum_{i=1}^{D} (x_i + 0.5)^2$	(-100, 100)	30	0
	f_7	$f_7(x) = \sum_{i=1}^{n} i x_i^4 + rand(0,1)$	(-1.28, 1.28)	30	0

TABLE 5. Multimodal benchmark functions for HHO-MSS benchmarking.

	No	Function	Search Space	*D*	f_{min}
Multimodal benchmark functions	f_8	$f_8(x) = \sum_{i=1}^{n} -x_i \sin(\sqrt{\lvert x_i \rvert})$	(500, 500)	30	-418.9 *n*
	f_9	$f_9(x) = \sum_{i=1}^{n} [x_i^2 - 10\cos(2\pi x_i) + 10]$	(5.12, 5.12)	30	0
	f_{10}	$f_{10}(x) = -20\exp\left(-0.2\sqrt{\frac{1}{n}\sum_{i=1}^{n} x_i^2}\right) - \exp\left(\frac{1}{n}\sum_{i=1}^{n} \cos(2\pi x_i)\right) + 20 + e$	(32, 32)	30	0
	f_{11}	$f_{11}(x) = \frac{1}{4000}\sum_{i=1}^{n} x_i^2 - \prod_{i=1}^{n} \cos\left(\frac{x_i}{\sqrt{i}}\right) + 1$	(600, 600)	30	0
	f_{12}	$f_{12}(x) = \frac{\pi}{n}\left\{10\sin(\pi y_1) + \sum_{i=1}^{n-1}(y_i - 1)^2[1 + 10\sin^2(\pi y_{i+1})] + (y_n - 1)^2\right\} + \sum_{i-1}^{n} u(x_i, 10, 100, 4)$ $y_i = 1 + \frac{x_i + 1}{4}$ $u(x_i, a, k, m) = \begin{cases} k(x_i - a)^m & x_i > a \\ 0 - a & < x_i < a \\ k(-x_i - a)^m & x_i < -a \end{cases}$	(50, 50)	30	0
	f_{13}	$f_{13}(x) = 0.1\left\{\sin^2(3\pi x_1) + \sum_{i=1}^{n}(x_1 - 1)^2[1 + \sin^2(3\pi x_1 + 1)] + (x_n - 1)^2[1 + \sin^2(2\pi x_n)]\right\}$ $+ \sum_{i=1}^{n} u(x_i, 5, 100, 4)$	(50, 50)	30	0

TABLE 6. Fixed dimension multimodal benchmark functions for HHO-MSS benchmarking.

	No	Function	Search Space	D	f_{min}
Fixed dimension multiodal benchmark functions	f_{14}	$f_{14}(x) = \left(\frac{1}{500} + \sum_{j=1}^{25} \frac{1}{j + \sum_{i=1}^{2}(x_i - a_{ij})^6}\right)^{-1}$	(-65, 65)	2	1
	f_{15}	$f_{15}(x) = \sum_{i=1}^{11}\left[a_i - \frac{x_1(b_i^2 + b_i x_2)}{b_i^2 + b_i x_3 + x_4}\right]^2$	(-5, 5)	4	0.0003
	f_{16}	$f_{16}(x) = 4x_1^2 - 2.1x_1^4 + \frac{1}{3}x_1^6 + x_1x_2 - 4x_2^2 + 4x_2^4$	(-5, 5)	2	-1.0316
	f_{17}	$f_{17}(x) = (x_2 - \frac{5.1}{4\pi^2}x_1^2 + \frac{5}{\pi}x_1 - 6)^2 + 10\left(1 - \frac{1}{8\pi}\right)cosx_1 + 10$	(-5, 5)	2	0.398
	f_{18}	$f_{18}(x) = [1 + (x_1 + x_2 + 1)^2(19 - 14x_1 + 3x_1^2 - 14x_2 + 6x_1x_2 + 3x_2^2)] \times [30 + (2x_1 - 3x_2)^2 \times (18 - 32x_1 + 12x_1^2 + 48x_2 - 36x_1x_2 + 27x_2^2)]$	(-2, 2)	2	3
	f_{19}	$f_{19}(x) = -\sum_{i=1}^{4} c_i exp\left(-\sum_{j=1}^{3} a_{ij}(x_j - p_{ij})^2\right)$	(1, 3)	3	-3.86
	f_{20}	$f_{20}(x) = -\sum_{i=1}^{4} c_i exp\left(-\sum_{j=1}^{6} a_{ij}(x_j - p_{ij})^2\right)$	(0, 1)	6	-3.32
	f_{21}	$f_{21}(x) = -\sum_{i=1}^{5}[(X - a_i)(X - a_i)^T + c_i]^{-1}$	(0, 10)	4	-10.153
	f_{22}	$f_{22}(x) = -\sum_{i=1}^{7}[(X - a_i)(X - a_i)^T + c_i]^{-1}$	(0, 10)	4	-10.402
	f_{23}	$f_{22}(x) = -\sum_{i=1}^{10}[(X - a_i)(X - a_i)^T + c_i]^{-1}$	(0, 10)	4	-10.536

$$GCP = \begin{cases} 0.5r_7, & r_8 \geq GP \\ 0, & r_8 < GP \end{cases} \quad (60)$$

with the Generation Rate Control Parameter (GCP) defined as 0.5 and Generation Probability (GP) is a random value between 0 to 1. The r_7 and r_8 are random values 0 to 1

In the rest, HHO-MSS continues the hunting process until the maximum iteration or a terminated condition is reached.

IV. SIMULATION AND DISCUSSION

This section is divided into two parts: the first part focuses on the proposed algorithm benchmarking, and the second part presents the optimal parameters of PSS and VI in the dynamic stability of renewable microgrid power systems. The simulation and optimization are performed in MATLAB 2022b with the following device specifications: AMD Ryzen 5 5600H 3.3 GHz, dual-channel RAM DDR4 16 GB, and NVIDIA GeForce GTX 1650 4 GB.

A. HHO-MSS BENCHMARKING

The Friedman Ranking Test, a non-parametric statistical test, is performed to investigate the significant difference, consistency, and accuracy of the proposed algorithm. Furthermore, convergence and energy escaping curves are conducted to analyze the exploration and exploitation ability. The proposed algorithm is compared with the other schemes of modified HHO, basic HHO, and basic EO. The parameters used for algorithms are described in Table 3.

1) STATISTICAL ASSESSMENT

Using The Friedman Ranking Test, the statistical performances of HHO-MSS are carried out. This test uses three

TABLE 7. Friedman Ranking Test results for HHO-MSS benchmarking in fixed dimension multimodal benchmark functions.

Func.	Statistical Parameter	Algorithm				
		#1 Proposed HHO-MSS	#2 Iteration-based HHO-EO	#3 Population-based HHO-EO	#4 HHO	#5 EO
f_1	Min.	3.01E-32	1.70E-04	2.09E-05	5.77E-24	1.84E-27
	Max.	1.38E-24	2.38E-03	1.57E-04	1.28E-22	3.52E-23
	Avg.	2.76E-25	1.17E-03	6.28E-05	6.13E-23	7.20E-24
	Std.	6.15E-25	9.86E-04	5.77E-05	5.43E-23	1.56E-23
f_2	Min.	1.97E-15	1.82E-03	4.61E-03	3.41E-13	2.01E-14
	Max.	1.39E-13	3.46E-03	4.45E-02	1.87E-12	7.55E-11
	Avg.	3.53E-14	2.52E-03	1.67E-02	1.26E-12	1.60E-11
	Std.	5.83E-14	7.67E-04	1.58E-02	6.44E-13	3.33E-11
f_3	Min.	1.20E-26	3.50E-03	2.15E-03	6.79E-07	1.28E-24
	Max.	3.30E-16	3.23E-02	1.25E-02	1.96E-04	5.67E-17
	Avg.	6.60E-17	1.67E-02	6.49E-03	8.28E-05	1.17E-17
	Std.	1.48E-16	1.28E-02	4.61E-03	7.95E-05	2.52E-17
f_4	Min.	6.36E-16	1.01E-04	4.41E-03	3.44E-06	3.20E-14
	Max.	3.71E-12	3.34E-02	5.27E-02	7.46E-06	2.57E-11
	Avg.	1.16E-12	9.91E-03	2.12E-02	5.60E-06	5.28E-12
	Std.	1.60E-12	1.37E-02	1.94E-02	1.45E-06	1.14E-11
f_5	Min.	1.42E-04	3.43E-03	2.83E-03	2.57E-02	4.31E-05
	Max.	7.20E-03	3.33E-02	2.88E-02	2.61E-02	5.53E-02
	Avg.	3.26E-03	2.03E-02	1.82E-02	2.59E-02	2.45E-02
	Std.	3.35E-03	1.55E-02	1.40E-02	1.58E-04	2.76E-02
f_6	Min.	9.86E-05	2.55E-03	4.85E-03	1.56E-04	4.38E-04
	Max.	8.87E-03	4.34E-02	6.39E-02	4.05E-04	1.48E-02
	Avg.	2.55E-03	1.35E-02	2.78E-02	2.57E-04	3.38E-03
	Std.	3.71E-03	1.72E-02	2.48E-02	1.01E-04	6.36E-03
f_7	Min.	3.44E-05	6.69E-03	9.85E-05	1.16E-03	9.71E-05
	Max.	7.54E-04	2.02E-02	1.44E-03	2.25E-03	1.50E-03
	Avg.	3.71E-04	1.24E-02	4.58E-04	1.59E-03	6.97E-04
	Std.	3.43E-04	5.94E-03	5.61E-04	4.30E-04	5.65E-04
p-value		0.376	0.251	0.171	0.137	0.096
Friedman Ranking		1	2	3	4	5

sets of benchmark functions for algorithms as follows: unimodal benchmark functions as given in Table 4, multimodal benchmark functions as given in Table 5, and fixed dimension multimodal benchmark functions as given in Table 6. Each of the algorithms performs 30 runs to solve the benchmark functions.

The statistical results for unimodal benchmark functions are tabulated in Table 7. The unimodal benchmark functions aim to measure the ability of the algorithm in the exploitation process. The *p-value* indicates the significance of the difference in the optimization result based on statistical parameters. If *p-value*$\leq$ 0.05, then the obtained results are significantly difference. This condition indicates the variation level in the results is high. It means the algorithm with a *p-value*$\leq$ 0.05 has bad consistency. While *p-value*$>$ 0.05, then the obtained results are no significantly difference. It indicates the variation level in the results is low. It means the algorithm with a *p-value*$>$ 0.05 has good consistency. Thus, a higher *p-value* means a better consistency of the algorithm. From Table 7, it can be seen that HHO-MSS obtained the highest p-value by 0.376. The common hybrid version algorithms also give higher *p-value* than basic algorithms.

The statistical results for multimodal benchmark functions are given in Table 8. The multimodal benchmark functions test the ability of the algorithm in the exploration process. HHO-MSS has also shown a greater performance than the other compared algorithms. Based on Table 8, HHO-MSS is consistent in obtaining the highest *p-value* of 0.916. The common hybrid version algorithms show worse results than the basic HHO and EO. Besides that, statistical results for fixed dimension multimodal benchmark functions are provided in Table 9. The fixed dimension multimodal benchmark functions investigate the ability of the algorithm to solve low dimension optimization cases. The result shows a similar attribute to Table 8. The HHO-MSS offers the highest *p-value* of 0.979. The common hybrid version algorithms have also given worse results than the basic HHO and EO.

From Table 7, Table 8, and Table 9, it can be concluded that HHO-MSS has increased the overall performance than the basic HHO and EO. HHO-MSS offers superior ability in exploration, exploitation, and solving the low dimension optimization cases than the compared algorithms. On the other hand, the investigation has also proven that the common hybrid method of the algorithms did not always provide better results than the basic algorithms. Thus, it needs a specific scenario or scheme to enhance the overall performance of the algorithms.

The statistical results have concluded that HHO-MSS has better consistency and accuracy than the others. A proper metaheuristic algorithm must have good exploration and

TABLE 8. Friedman Ranking Test results for HHO-MSS benchmarking in multimodal benchmark functions.

Func.	Statistical Parameter	Algorithm				
		#1 Proposed HHO-MSS	#2 Iteration-based HHO-EO	#3 Population-based HHO-EO	#4 HHO	#5 EO
f_8	Min.	-1.26E+04	-1.26E+04	-7.66E+03	-8.99E+03	-6.62E+03
	Max.	-1.26E+04	-1.01E+04	-6.64E+03	-7.30E+03	-4.02E+03
	Avg.	-1.26E+04	-1.21E+04	-7.16E+03	-8.12E+03	-5.36E+03
	Std.	7.82E+00	1.09E+03	3.96E+02	6.51E+02	1.03E+03
f_9	Min.	0.00E+00	0.00E+00	2.47E-04	0.00E+00	5.68E-14
	Max.	0.00E+00	0.00E+00	1.20E+00	5.68E-14	3.41E-13
	Avg.	0.00E+00	0.00E+00	4.58E-01	2.27E-14	1.48E-13
	Std.	0.00E+00	0.00E+00	6.28E-01	3.11E-14	1.18E-13
f_{10}	Min.	4.00E-15	4.44E-16	8.05E-04	3.13E-13	9.28E-14
	Max.	2.03E-13	1.03E-13	1.76E-03	5.60E-12	1.32E-13
	Avg.	4.38E-14	5.02E-14	1.29E-03	2.23E-12	1.08E-13
	Std.	8.90E-14	3.82E-14	4.08E-04	2.40E-12	1.56E-14
f_{11}	Min.	0.00E+00	0.00E+00	5.51E-05	0.00E+00	2.44E-15
	Max.	0.00E+00	0.00E+00	3.58E-02	0.00E+00	3.44E-02
	Avg.	0.00E+00	0.00E+00	1.41E-02	0.00E+00	1.11E-02
	Std.	0.00E+00	0.00E+00	1.91E-02	0.00E+00	1.59E-02
f_{12}	Min.	1.62E-05	2.13E-05	1.58E-02	1.26E-05	2.61E-02
	Max.	5.38E-04	4.68E-04	3.20E-02	2.85E-05	9.91E-02
	Avg.	1.72E-04	2.22E-04	2.50E-02	2.09E-05	6.82E-02
	Std.	2.12E-04	1.70E-04	7.66E-03	5.69E-06	3.32E-02
f_{13}	Min.	1.77E-04	3.30E-04	4.77E-01	8.73E-03	4.28E-01
	Max.	7.14E-03	6.06E-03	9.40E-01	2.10E-01	8.32E-01
	Avg.	3.21E-03	2.82E-03	7.29E-01	1.12E-01	6.05E-01
	Std.	2.73E-03	2.24E-03	1.66E-01	9.71E-02	1.57E-01
p-value		0.916	0.139	0.043	0.603	0.562
Friedman Ranking		1	4	5	2	3

exploitation abilities because these features can validate the obtained results when the algorithm is implemented in real cases. From the statistical results, the HHO-MSS is considered a reliable algorithm to be implemented in controlling the parameters of PSS and VI.

2) CONVERGENCE AND ENERGY ESCAPING CURVES ANALYSIS

The process of the algorithm in obtaining the best solution can be drawn in the convergence curve. This curve gives the history of the best solution in each iteration. The normalized average convergence curve of the investigated algorithms in 30 runs in solving the benchmark functions is figured in Figure 10. It can be seen that EO has a better convergence curve than HHO. However, HHO can offer better solutions. It shows that the HHO and EO have their superiority. Second, Iteration-based HHO-EO and Population-based HHO-EO have better curves than HHO and EO. However, the convergence curve analysis gives different perspectives. The curve of Iteration-based HHO-EO tends to be similar to HHO in initial iterations, and it can be similar to EO in the rest. While the Population-based HHO-EO gives more random characteristics than the other one. Furthermore, it can be seen that HHO-MSS has the best convergence curve. The characteristic of the curve is a bit different than the others. It has also converged faster into its optimal solutions and seems to have a better ability to avoid local optima. This investigation justifies the superiority of the new scheme of enhanced HHO-MSS over the others.

The comparison of the average energy escaping curve between HHO and HHO-MSS is given in Figure 11. The energy escaping curve in HHO represents the exploration and exploitation process. The proportion of the exploration and exploitation can be investigated using the trend line (marked by the red line in Figure 11) and *R-squared* parameter. The *R-squared* value represents the goodness of fit of the variations in the escaping energy curve. A higher *R-squared* value means better variety in the exploration and exploitation processes. The results indicate the process of finding a solution in the algorithm does not dwell on one side, it could be dwell on the exploration or exploitation. Thus, a higher *R-squared* value means a better proportion of exploration and exploitation. It can be seen in Figure 11 that HHO-MSS has a significantly higher *R-squared* value than basic HHO in all of the benchmark functions. It can be concluded that the proposed scheme makes the exploration and exploitation process run better.

B. OPTIMAL PARAMETERS FOR PSS AND VI

The investigation in controlling the parameters of PSS and VI has used the power system parameters and the default parameters of dual-input PSS as given in Table 10 and Table 11, respectively. Then, the renewable microgrid power system simulation is conducted in several scenarios to analyze the renewable microgrid behavior in various RES penetrations

TABLE 9. Friedman Ranking Test results for HHO-MSS benchmarking in unimodal benchmark functions.

Func.	Statistical Parameter	Algorithm				
		#1 Proposed HHO-MSS	#2 Iteration-based HHO-EO	#3 Population-based HHO-EO	#4 HHO	#5 EO
f_{14}	Min.	9.98E-01	9.98E-01	9.98E-01	9.98E-01	9.98E-01
	Max.	3.97E+00	9.98E-01	1.99E+00	2.98E+00	5.93E+00
	Avg.	2.19E+00	9.98E-01	1.20E+00	1.39E+00	1.98E+00
	Std.	1.08E+00	0.00E+00	4.45E-01	8.87E-01	2.21E+00
f_{15}	Min.	3.60E-04	6.62E-04	4.12E-04	3.10E-04	3.71E-04
	Max.	7.66E-04	2.04E-02	2.04E-02	6.74E-04	4.56E-04
	Avg.	6.37E-04	4.73E-03	4.54E-03	5.54E-04	4.17E-04
	Std.	1.72E-04	8.74E-03	8.84E-03	1.42E-04	3.02E-05
f_{16}	Min.	-1.03E+00	-1.03E+00	-1.03E+00	-1.03E+00	-1.03E+00
	Max.	-1.03E+00	-1.03E+00	-1.03E+00	-1.03E+00	-1.03E+00
	Avg.	-1.03E+00	-1.03E+00	-1.03E+00	-1.03E+00	-1.03E+00
	Std.	0.00E+00	0.00E+00	0.00E+00	0.00E+00	0.00E+00
f_{17}	Min.	3.98E-01	3.98E-01	3.98E-01	3.98E-01	3.98E-01
	Max.	3.98E-01	3.98E-01	3.98E-01	4.00E-01	3.98E-01
	Avg.	3.98E-01	3.98E-01	3.98E-01	3.98E-01	3.98E-01
	Std.	1.15E-06	8.94E-11	0.00E+00	9.47E-04	2.24E-05
f_{18}	Min.	3.00E+00	3.00E+00	3.00E+00	3.00E+00	3.00E+00
	Max.	3.00E+00	3.00E+00	3.00E+00	3.00E+00	3.00E+00
	Avg.	3.00E+00	3.00E+00	3.00E+00	3.00E+00	3.00E+00
	Std.	0.00E+00	0.00E+00	1.52E-04	0.00E+00	1.17E-03
f_{19}	Min.	-3.86E+00	-3.86E+00	-3.86E+00	-3.86E+00	-3.86E+00
	Max.	-3.86E+00	-3.86E+00	-3.85E+00	-3.86E+00	-3.77E+00
	Avg.	-3.86E+00	-3.86E+00	-3.86E+00	-3.86E+00	-3.84E+00
	Std.	8.94E-10	0.00E+00	3.40E-03	2.89E-03	3.69E-02
f_{20}	Min.	-3.32E+00	-3.32E+00	-3.32E+00	-3.13E+00	-3.07E+00
	Max.	-3.20E+00	-3.09E+00	-3.11E+00	-2.92E+00	-2.81E+00
	Avg.	-3.27E+00	-3.23E+00	-3.23E+00	-3.01E+00	-2.96E+00
	Std.	6.51E-02	9.86E-02	9.20E-02	7.97E-02	1.02E-01
f_{21}	Min.	-1.02E+01	-1.02E+01	-1.02E+01	-5.00E+00	-9.07E+00
	Max.	-2.68E+00	-2.63E+00	-5.06E+00	-4.81E+00	-5.01E+00
	Avg.	-7.64E+00	-6.61E+00	-9.13E+00	-4.93E+00	-5.84E+00
	Std.	3.54E+00	3.38E+00	2.28E+00	7.41E-02	1.81E+00
f_{22}	Min.	-1.04E+01	-1.04E+01	-1.04E+01	-5.09E+00	-5.06E+00
	Max.	-1.84E+00	-2.75E+00	-1.04E+01	-4.92E+00	-2.73E+00
	Avg.	-7.16E+00	-6.28E+00	-1.04E+01	-5.02E+00	-4.57E+00
	Std.	4.45E+00	3.88E+00	2.94E-03	8.28E-02	1.03E+00
f_{23}	Min.	-1.05E+01	-1.05E+01	-1.05E+01	-8.92E+00	-9.27E+00
	Max.	-2.42E+00	-2.42E+00	-1.05E+01	-5.07E+00	-5.06E+00
	Avg.	-7.57E+00	-8.91E+00	-1.05E+01	-5.86E+00	-5.93E+00
	Std.	4.09E+00	3.63E+00	2.22E-03	1.71E+00	1.87E+00
p-value		0.979	0.387	0.001	0.547	0.415
Friedman Ranking		1	4	5	2	3

as given in Table 12. The small disturbance is represented by the sudden increase in the load power demand (ΔP_L). The simulation scenario is arranged based on renewable microgrid behavior in adjusting the net power generation (P_t) with various generation resources.

The different effects of RES penetrations are described in Figure 12 and Table 13. It shows that $\Delta P_L = 0.02$ p.u. at 2 s inflicts a RoCoF by -1.69 $\times$ 10^{-3} (-0.17% from steady state point) at 2.85 s. Then, the RES penetration makes the maximum overshoot different due to the PVES and WTES having different time responses. A higher RES penetration gives a higher maximum overshoot value. After the turning point, it shows that higher RES penetration gives more dampening effect in Δf response. Moreover, RES penetration can make the settling time faster. The different effects of various RES conditions make the controlling parameters of PSS and VI need a different treatment.

1) OPTIMAL PARAMETER RESULTS

The optimal controlling parameters for PSS and VI are detailed in Table 14. Then, the average normalized $f_{benson's}$ in the convergence curve is shown in Figure 13. It can be seen that the different algorithm gives optimal configuration variation based on RES penetration. HHO-MSS gives a superior result in average fitness value based on f_{benson}. The best average fitness value obtained by HHO-MSS is better than Iteration-based HHO-EO, Population-based HHO-EO, HHO, and EO of 9.63%, 13.79%, 22.55%, and 26.57%, respectively. It can be concluded that the different optimal parameters give different characteristics in Δf improvement.

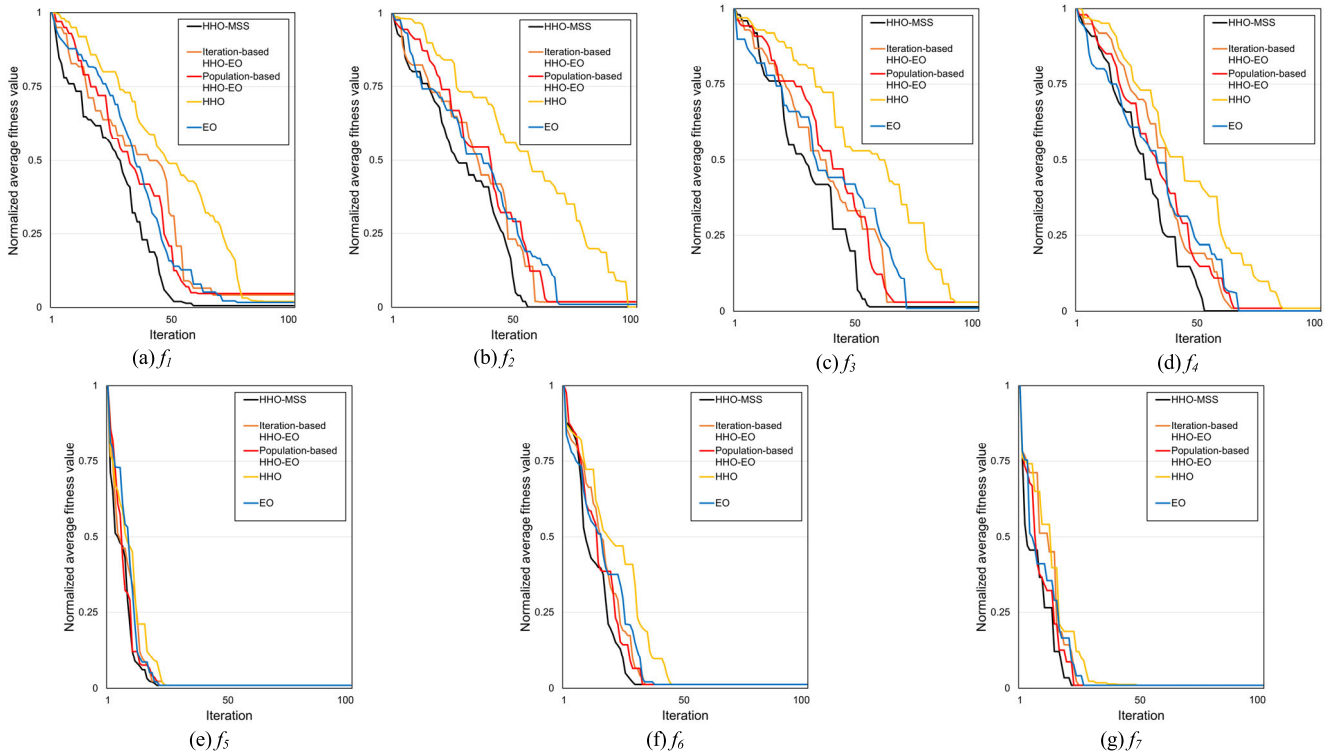

FIGURE 10. The comparison of the average convergence curve of the algorithms in benchmark functions.

TABLE 10. Summary of power system simulation parameters [4], [8].

Parameter	Value	Note
T_t	0.53	Turbine time response
T_g	0.28	Governor time response
R_D	19.6	Droop
β	20.13	Bias factor
K_S	0.1	Control unit constant
T_{WT}	1.4	WT time response
T_{PV}	1.9	PV time response
k_A	50	Amplifier gain constant
T_A	0.05	Amplifier time constant
T'_{do}	5.9	Exciter time constant
K_1	1.36	
K_2	0.91	
K_3	0.42	Heffron-Phillips
K_4	1.69	constants
K_5	0.05	
K_6	0.66	
H	6.5	Base inertia value of the system
D	0.6	Base damping value of the system

TABLE 11. Summary of default parameters in dual-input PSS [56].

Parameter	Value	Note
K_{PSS2}	$K_{PSS2} = \frac{T_7}{2H}$	PSS gain constants
K_{PSS3}	1	
T_{W1}	10	
T_{W2}	10	Wash-out filter constants
T_{W3}	10	
T_{W4}	usually bypassed	
T_6	0	Lag control time constants
T_7	$T_7 = T_{W2}$	
T_8	0.3	
T_9	0.15	Ramp-tracking features
M	2	
N	4	

TABLE 12. Simulation scenarios for renewable microgrid power system.

RES Penetration	ΔP_L	ΔP_e	ΔP_{WT}	ΔP_{PV}
	p.u.			
#1 Low (10%)	0.02	0.018	0.001	0.001
#2 Mid (50%)		0.01	0.005	0.005
#3 High (75%)		0.005	0.0075	0.0075
#4 Full (100%)		-	0.01	0.01

2) EIGENVALUE ANALYSIS

In this paper, the problem formulation is constructed using a combination of damping factor and damping ratio that is related to the eigenvalue of the system. Thus, the eigenvalue of the system in different RES penetrations is given in Table 15. The dynamic stability improvement can be indicated by the shifting of the eigenvalue point to the left side. It means the real part of the eigenvalue becomes more negative.

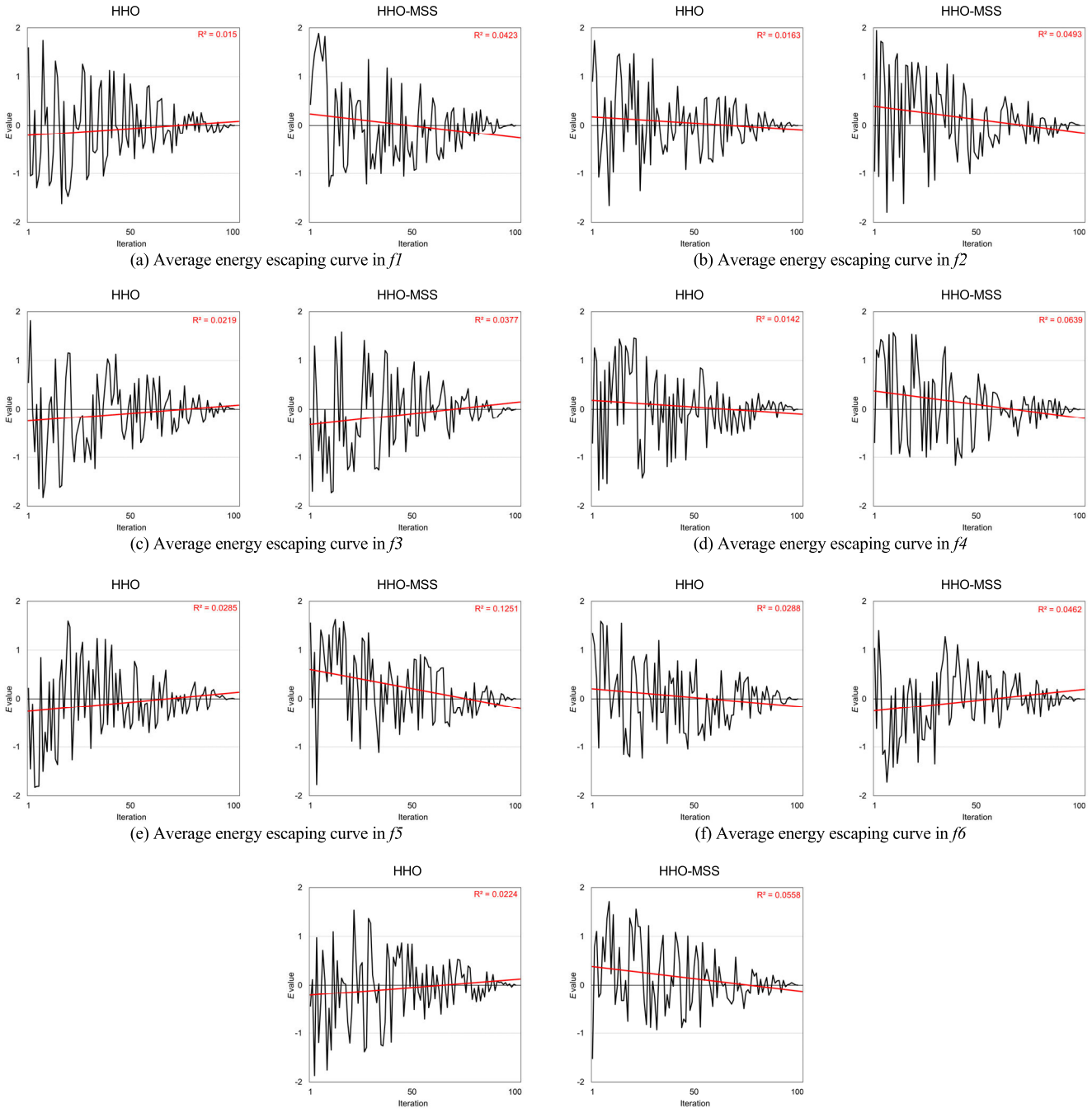

(a) Average energy escaping curve in *f1*
(b) Average energy escaping curve in *f2*
(c) Average energy escaping curve in *f3*
(d) Average energy escaping curve in *f4*
(e) Average energy escaping curve in *f5*
(f) Average energy escaping curve in *f6*
(g) Average energy escaping curve in *f7*

FIGURE 11. **The comparison of the energy escaping curve of the rabbit between HHO and HHO-MSS.**

From Table 15, PSS is more effective in giving a damping effect than VI in low and mid RES penetrations. In low RES penetrations, PSS with HHO-MSS gives an eigenvalue of -14.4697 ± 2.8296i, which is more negative than VI with HHO-MSS of -10.2103 ± 4.0331i. Moreover, the PSS-VI with HHO-MSS gives the most negative value in low RES penetration of -14.5946 ± 3.1050i. Similar to mid RES penetrations, PSS also gives a better damping effect. It can be seen the eigenvalue by PSS with HHO-MSS is -10.2115 ± 4.0352i, which is more negative than VI with HHO-MSS of -5.7235 ± 2.4094i. Moreover, the PSS-VI with HHO-MSS gives the most negative value in mid RES penetration of -10.7631 ± 4.4868i.

Based on eigenvalue analysis, the effectiveness between PSS or VI in high and full RES penetrations is reversed compared to low and mid RES penetrations. In high and full RES penetrations, the VI seems to have more impact in improving the stability than the PSS. In high RES penetrations, it can

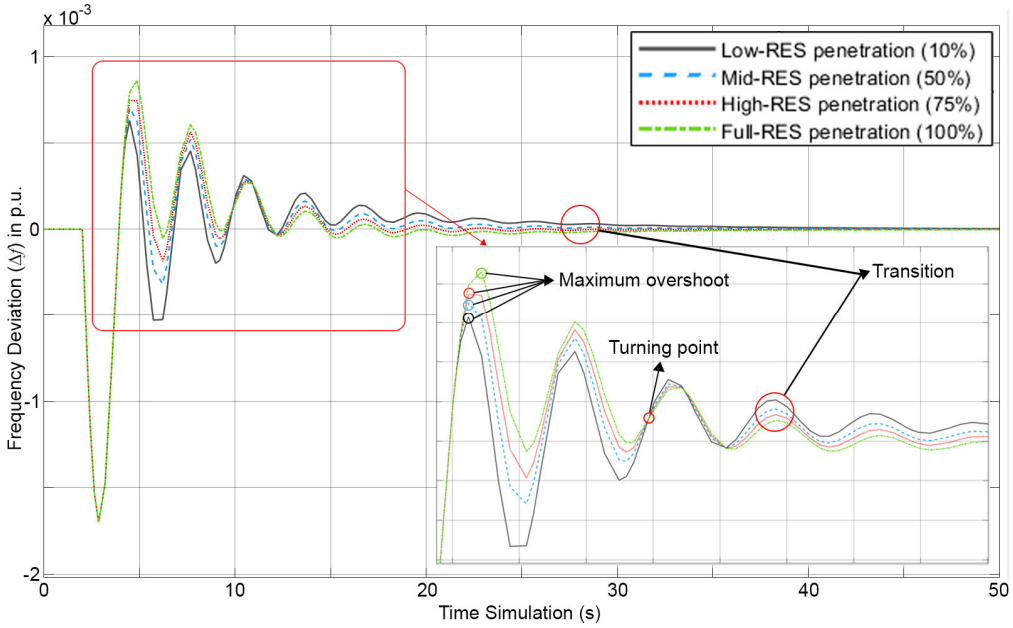

FIGURE 12. Effect on Δf in various RES penetrations (base case).

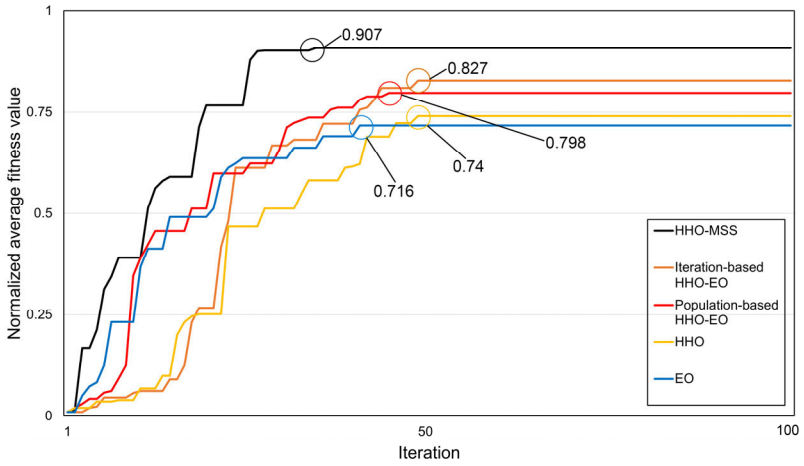

FIGURE 13. Average normalized $f_{benson's}$.

TABLE 13. Detailed Δf in various RES penetrations (base case).

Parameter	RES Penetration Condition			
	#1 Low (10%)	#2 Mid (50%)	#3 High (75%)	#4 Full (100%)
Freq. nadir	-1.69 x 10^{-3} (-0.17% from steady state point)			
Overshoot	0.063%	0.071%	0.074%	0.086%
Settling time	13.764 s	11.144 s	11.165 s	11.196 s

be seen that VI with HHO-MSS gives the eigenvalue of -13.7411 ± 5.9938i, which is better than PSS with HHO-MSS of -10.2113 ± 4.0348i. Moreover, the PSS-VI with HHO-MSS gives the most negative value in high RES penetration of -13.7649 ± 6.1301i. In full RES penetrations, the VI with HHO-MSS conducts the eigenvalue of -11.3492 ± 3.3669i, which is more negative than PSS with HHO-MSS of -10.2115 ± 4.0352i. Moreover, the PSS-VI with HHO-MSS gives the most negative value in full RES penetration of -11.4791 ± 3.3182i. Then, the eigenvalue analysis can be strengthened by time domain simulation analysis in RES penetrations in the following.

3) TIME DOMAIN SIMULATION: LOW-RES SCENARIO

The frequency deviation (Δf) and power angle deviation ($\Delta\delta$) responses in low-RES penetration are shown in

TABLE 14. Optimal parameter results for PSS and VI in renewable microgrid power system.

RES Penetration	Algorithm	Optimal Parameter							Normalized $f_{benson's}$
		K_{PSS}	T_1	T_2	T_3	T_4	K_{VI}	D_{VI}	
Low	HHO-MSS	9.058	0.038	0.146	0.147	0.064	0.101	1.932	0.956
	Iteration-based HHO-EO	9.326	0.023	0.018	0.013	0.01	0.669	1.92	0.873
	Population-based HHO-EO	9.997	0.069	0.168	0.036	0.298	0.921	1.572	0.814
	HHO	10	0.049	0.145	0.01	0.182	0.573	1.475	0.789
	EO	10	0.011	0.2	0.017	0.018	0.27	0.161	0.742
Mid	HHO-MSS	10	0.199	0.2	0.187	0.194	3.079	1.982	0.92
	Iteration-based HHO-EO	10	0.182	0.185	0.097	0.2	1.096	2	0.852
	Population-based HHO-EO	9.610	0.141	0.05	0.084	0.179	0.116	1.992	0.829
	HHO	9.992	0.026	0.188	0.128	0.2	0.536	1.89	0.748
	EO	9.867	0.067	0.121	0.021	0.164	0.117	1.976	0.731
High	HHO-MSS	8.744	0.03	0.026	0.15	0.141	0.256	1.668	0.898
	Iteration-based HHO-EO	9.875	0.013	0.065	0.036	0.067	0.276	1.675	0.836
	Population-based HHO-EO	10	0.05	0.055	0.044	0.2	0.101	1.99	0.824
	HHO	4.569	0.098	0.134	0.168	0.2	0.1	0.784	0.727
	EO	4.725	0.2	0.118	0.027	0.186	0.133	0.1	0.71
Full	HHO-MSS	10	0.012	0.038	0.087	0.158	2.948	1.993	0.856
	Iteration-based HHO-EO	10	0.01	0.196	0.074	0.143	1.273	1.189	0.75
	Population-based HHO-EO	9.939	0.061	0.2	0.17	0.203	0.189	2	0.723
	HHO	9.297	0.026	0.182	0.062	0.186	1.275	1.152	0.698
	EO	9.15	0.01	0.179	0.01	0.183	1.273	1.152	0.685

TABLE 15. Eigenvalue of the system in various RES penetrations.

PSS HHO-MSS	VI HHO-MSS	PSS+VI HHO-MSS	PSS+VI Iteration-based HHO-EO	PSS+VI Population-based HHO-EO	HHO	EO
Low-RES Penetration						
-14.4697 + 2.8296i	-10.2103 + 4.0331i	-14.5946 + 3.1050i	-11.6932 + 4.8281i	-10.1178 + 4.3524i	-9.9981 + 5.1926i	-11.2914 + 4.7297i
-14.4697 - 2.8296i	-10.2103 - 4.0331i	-14.5946 - 3.1050i	-11.6932 - 4.8281i	-10.1178 - 4.3524i	-9.9981 - 5.1926i	-11.2914 - 4.7297i
Mid-RES Penetration						
-10.2115 + 4.0352i	-5.7235 + 2.4094i	-10.7631 + 4.4868i	-10.7094 + 3.3554i	-9.1071 + 3.0666i	-5.4957 + 2.8254i	-10.5876 + 5.1430i
-10.2115 - 4.0352i	-5.7235 - 2.4094i	-10.7631 - 4.4868i	-10.7094 - 3.3554i	-9.1071 - 3.0666i	-5.4957 - 2.8254i	-10.5876 - 5.1430i
High-RES Penetration						
-10.2113 + 4.0348i	-13.7411 + 5.9938i	-13.7649 + 6.1301i	-6.3543 + 2.9318i	-11.1703 + 4.4396i	-10.4380 + 3.4908i	-11.5626 + 4.3172i
-10.2113 - 4.0348i	-13.7411 - 5.9938i	-13.7649 - 6.1301i	-6.3543 - 2.9318i	-11.1703 - 4.4396i	-10.4380 - 3.4908i	-11.5626 - 4.3172i
Full-RES Penetration						
-10.2115 + 4.0352i	-11.3492 + 3.3669i	-11.4791 + 3.3182i	-10.2828 + 4.8522i	-10.8686 + 4.0940i	-10.0658 + 4.6025i	-9.4599 + 5.1659i
-10.2115 - 4.0352i	-11.3492 - 3.3669i	-11.4791 - 3.3182i	-10.2828 - 4.8522i	-10.8686 - 4.0940i	-10.0658 - 4.6025i	-9.4599 - 5.1659i

TABLE 16. Detailed response in low-RES penetration with PSS and VI.

Parameter	Method						
	PSS HHO-MSS	VI HHO-MSS	PSS+VI HHO-MSS	PSS+VI Iter-based HHO-EO	PSS+VI Pop-based HHO-EO	PSS+VI HHO	PSS+VI EO
Freq. nadir (%)	-0.11	-0.135	-0.094	-0.095	-0.103	-0.106	-0.117
Δf Overshoot (p.u.)	-1.92×10^{-4}	1.08×10^{-4}	-2.78×10^{-4}	-2.26×10^{-4}	-4.30×10^{-5}	-6.71×10^{-5}	-2.82×10^{-5}
Δf Settling time (s)	5.453	6.114	5.515	5.546	5.72	5.464	5.406
$\Delta\delta$ Overshoot (p.u.)	1.7×10^{-2}	2.38×10^{-2}	1.47×10^{-2}	1.51×10^{-2}	1.67×10^{-2}	1.62×10^{-2}	1.75×10^{-2}
$\Delta\delta$ Settling time (s)	13.083	21.177	11.112	11.067	11.097	11.299	12.011

Figure 14 and Figure 15. An in-depth analysis focusing on Δf. $\Delta\delta$ is conducted to show that the Δf improvement is correlated to $\Delta\delta$. The detailed response in statistics is described in Table 16. From Figure 14, it can be seen that the

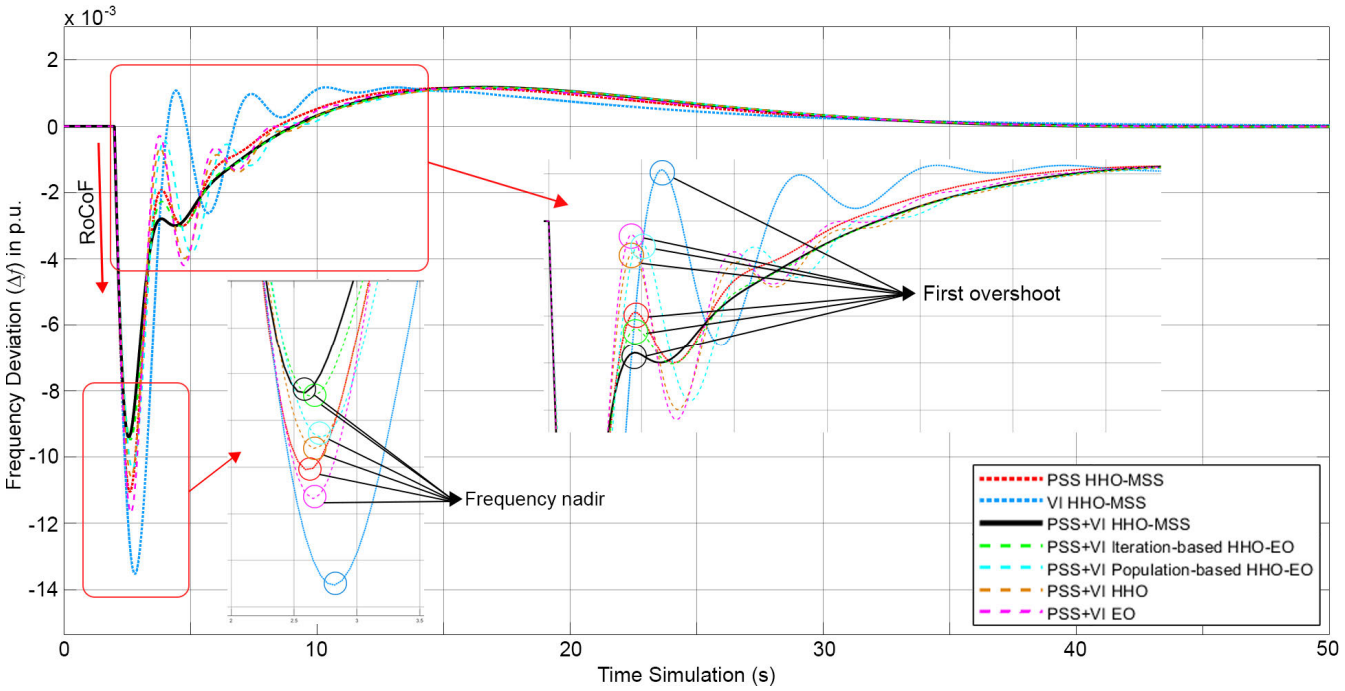

FIGURE 14. Δf response in low-RES penetration with PSS and VI.

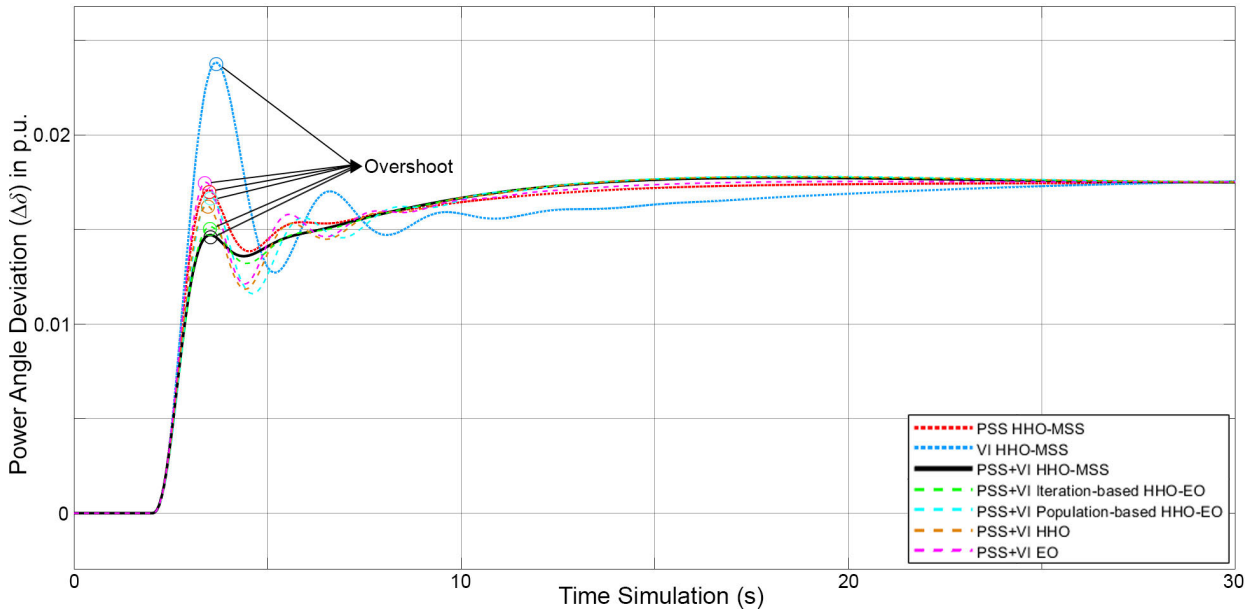

FIGURE 15. $\Delta\delta$ response in low-RES penetration with PSS and VI.

$\Delta P_L = 0.02$ p.u. at 2 s drops the frequency nadir. However, the PSS and VI can improve Δf by reducing the RoCoF and the minimum value of frequency nadir. In low-RES penetration, the effect of PSS is better than VI in improving dynamic stability.

A better improvement in frequency nadir is conducted by PSS of 35.3% than VI of 20.59% from the base case. When PSS and VI are combined, it can give better improvement. The improvement by HHO-MSS, Iteration-based HHO-EO, Population-based HHO-EO, HHO, and EO are 44.70%, 44.11%, 39.41%, 37.64%, and 31.17%, respectively. PSS gives a better dampening effect than the VI in the first overshoot. Besides that, the controlling parameters of PSS and VI by HHO-MSS give the lowest overshoot and the smoothest response. However, a smoother response can expense a longer settling time. Although it can be tolerated since the settling

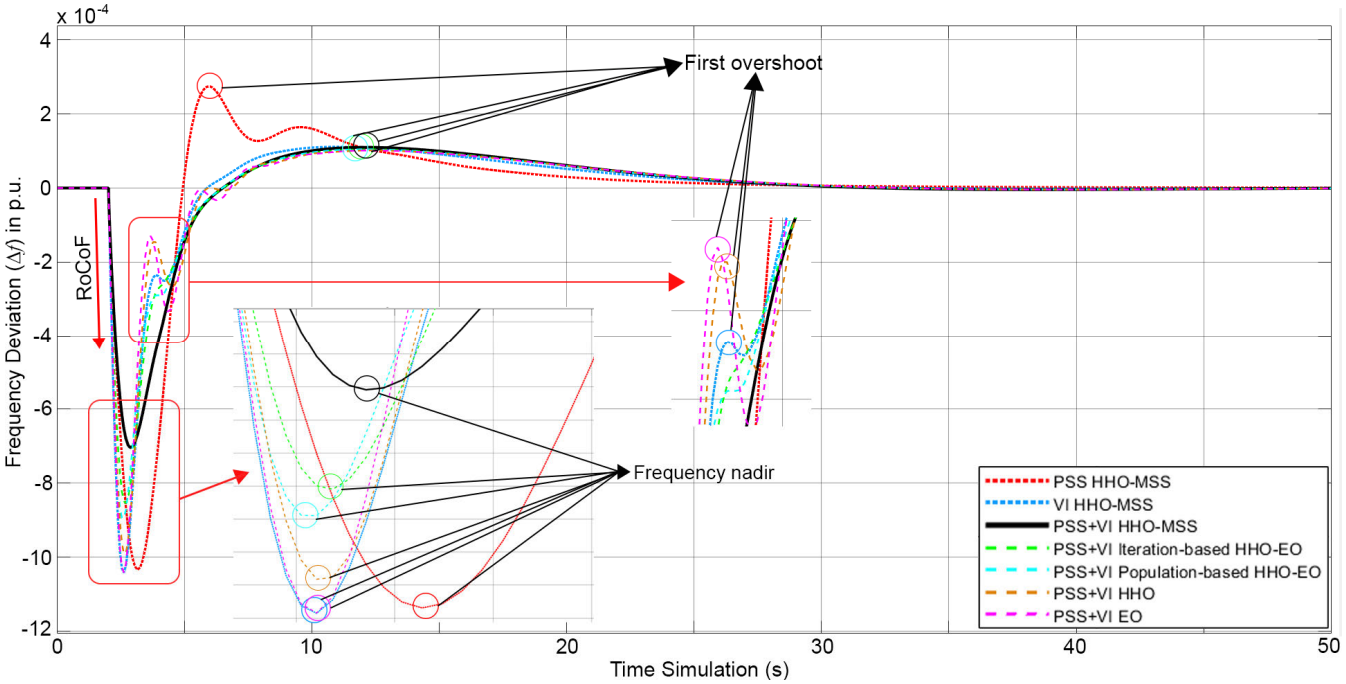

FIGURE 16. Δf response in mid-RES penetration with PSS and VI.

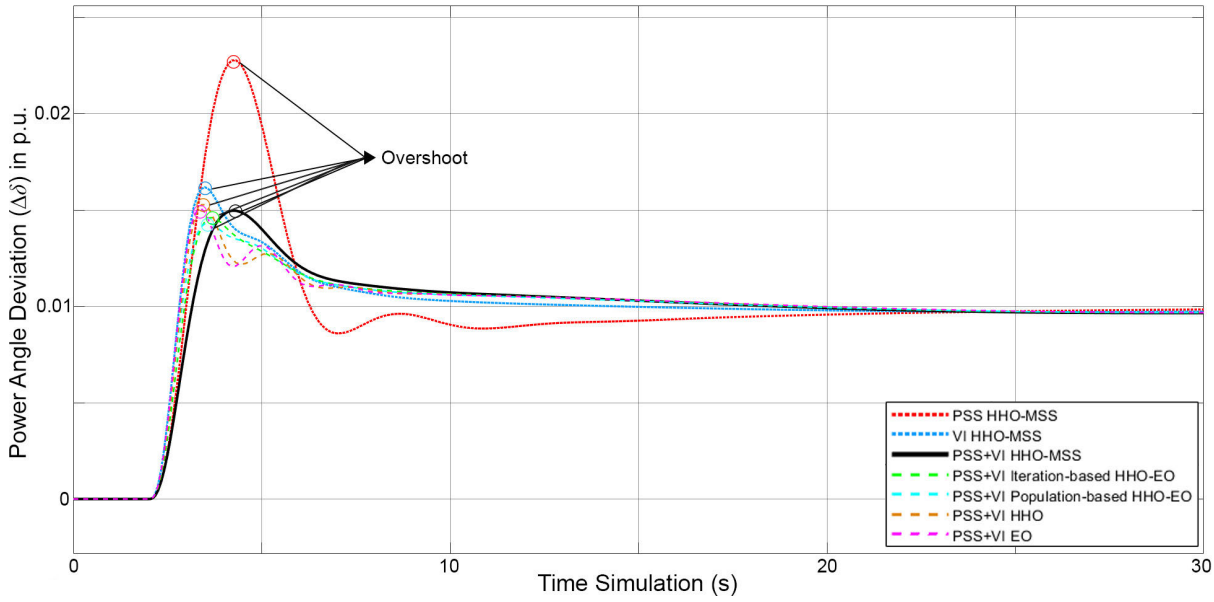

FIGURE 17. $\Delta\delta$ response in mid-RES penetration with PSS and VI.

time difference is very small. The improvement in the Δf is in line with the $\Delta\delta$. The PSS and VI parameters by HHO-MSS give the best overshoot reduction. From the investigating result, it can be concluded that PSS is more effective than VI for improving dynamic stability in low-RES penetration. Besides that, the overall result shows that the controlling parameters of PSS and VI by HHO-MSS offer the best improvement in frequency nadir, reducing overshoot, and refining the Δf and $\Delta\delta$ in low-RES penetration.

4) TIME DOMAIN SIMULATION: MID-RES SCENARIO

The Δf and $\Delta\delta$ responses in mid-RES penetration with PSS and VI are shown in Figure 16 and Figure 17. The detailed statistics are described in Table 17. In mid-RES penetration, the oscillation is harder to dampen. PSS has a better improvement of 39.41% than VI which gives a similar result of 38.82%. The controlling parameters of PSS and VI in mid-RES penetration show that HHO-MSS offers the best frequency nadir reduction of 58.82%, followed by

TABLE 17. Detailed response in mid-RES penetration with PSS and VI.

Parameter	Method						
	PSS HHO-MSS	VI HHO-MSS	PSS+VI HHO-MSS	PSS+VI Iter-based HHO-EO	PSS+VI Pop-based HHO-EO	PSS+VI HHO	PSS+VI EO
Freq. nadir (%)	-0.103	-0.104	-0.07	-0.085	-0.089	-0.099	-0.104
Δf Overshoot (p.u.)	2.74×10^{-4}	-1.09×10^{-4}	1.1×10^{-4}	1.04×10^{-4}	1.05×10^{-4}	-1.44×10^{-4}	-1.32×10^{-4}
Δf Settling time (s)	6.768	4.614	4.723	4.609	4.643	4.835	4.909
$\Delta\delta$ Overshoot (p.u.)	2.28×10^{-2}	1.62×10^{-2}	1.49×10^{-2}	1.46×10^{-2}	1.43×10^{-2}	1.53×10^{-2}	1.5×10^{-2}
$\Delta\delta$ Settling time (s)	5.909	5.856	6.083	5.754	5.731	5.763	5.624

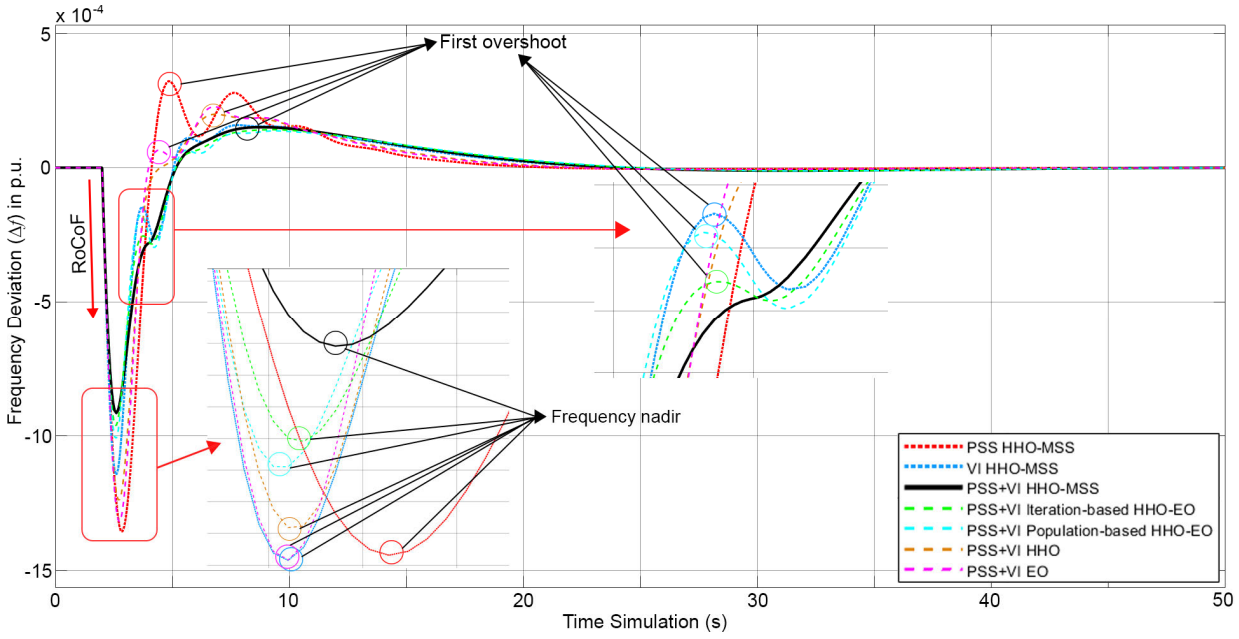

FIGURE 18. Δf response in high-RES penetration with PSS and VI.

TABLE 18. Detailed response in high-RES penetration with PSS and VI.

Parameter	Method						
	PSS HHO-MSS	VI HHO-MSS	PSS+VI HHO-MSS	PSS+VI Iter-based HHO-EO	PSS+VI Pop-based HHO-EO	PSS+VI HHO	PSS+VI EO
Freq. nadir (%)	-0.135	-0.114	-0.091	-0.096	-0.101	-0.124	-0.132
Δf Overshoot (p.u.)	3.22×10^{-4}	-1.47×10^{-4}	1.5×10^{-4}	-2.54×10^{-4}	-1.75×10^{-4}	2.01×10^{-4}	6.56×10^{-4}
Δf Settling time (s)	8.613	4.594	4.418	4.526	4.626	6.795	6.303
$\Delta\delta$ Overshoot (p.u.)	2.43×10^{-2}	1.68×10^{-2}	1.52×10^{-2}	1.48×10^{-2}	1.48×10^{-2}	2.05×10^{-2}	2.18×10^{-2}
$\Delta\delta$ Settling time (s)	7.344	8.462	8.959	9.338	9.534	7.335	7.120

Iteration-based HHO-EO, Population-based HHO-EO, HHO, and EO of 47.68%, 41.76%, and 38.82%, respectively. The improvement also impacted the $\Delta\delta$. The overshoot can be reduced properly using the PSS and VI parameters from HHO-MSS.

In mid-RES penetration, VI has a more significant contribution in dampening the overshoot than PSS. Besides that, the different optimal parameters of PSS and VI give more variation characteristics in mid-RES than low-RES penetration which tend to be similar. For example, PSS HHO-MSS,

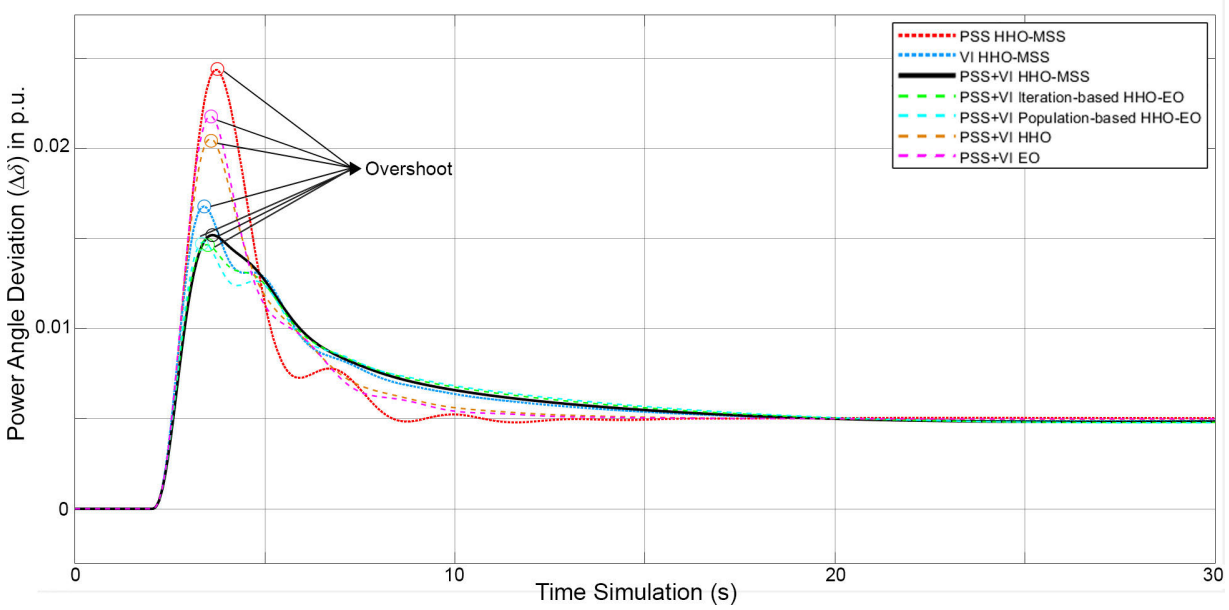

FIGURE 19. $\Delta\delta$ response in high-RES penetration with PSS and VI.

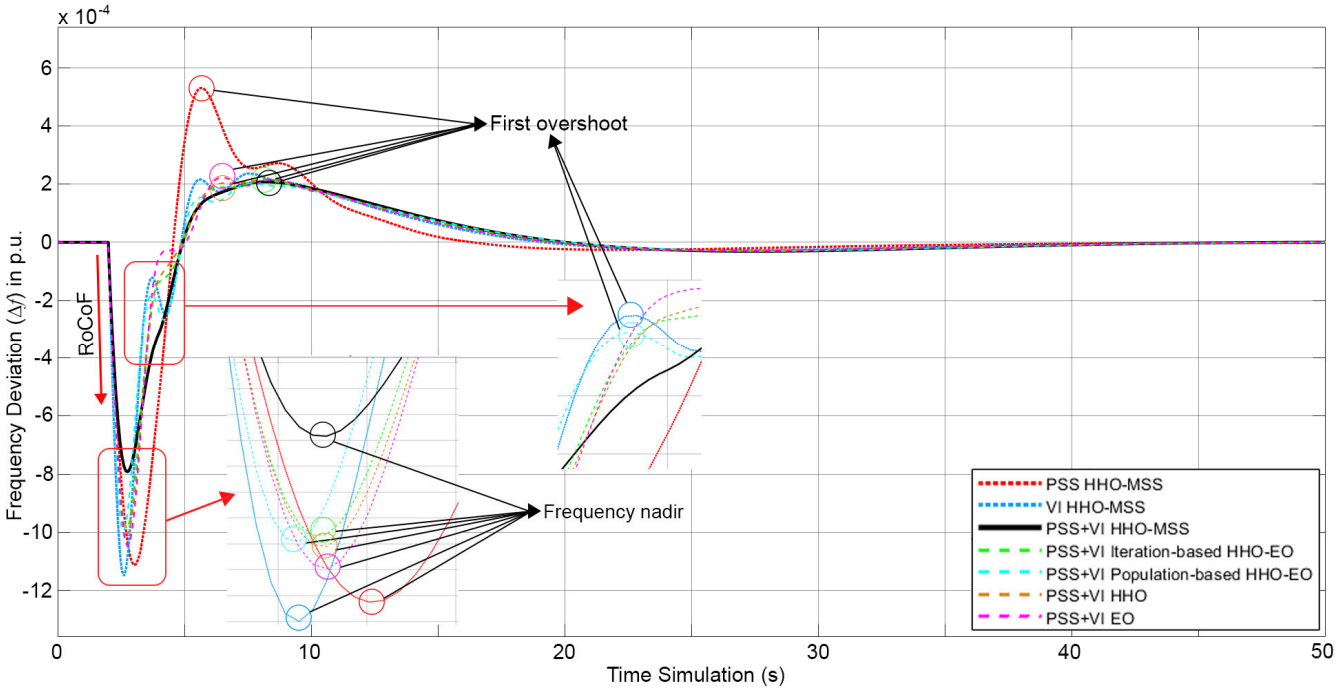

FIGURE 20. Δf response in full-RES penetration with PSS and VI.

PSS+VI HHO, and PSS+VI EO have the first overshoot under the steady state point. It means that configurations are a bit overdamped. On the other hand, PSS+VI HHO-MSS, PSS+VI Iteration-based HHO-EO, and PSS+VI Population-based offer smoother responses whereas the settling time becomes a bit longer. It can be seen that PSS is no longer effective in dampening the overshoot in mid-RES penetration. From the investigation result, the controlling parameters of PSS and VI by HHO-MSS give a significant improvement in both Δf and $\Delta\delta$ rather than the other algorithms.

5) TIME DOMAIN SIMULATION: HIGH-RES SCENARIO

The Δf and $\Delta\delta$ responses in high-RES penetration are shown in Figure 18 and Figure 19. The detailed response is described in Table 18. The higher the RES penetration level, the less effective PSS in improving dynamic stability.

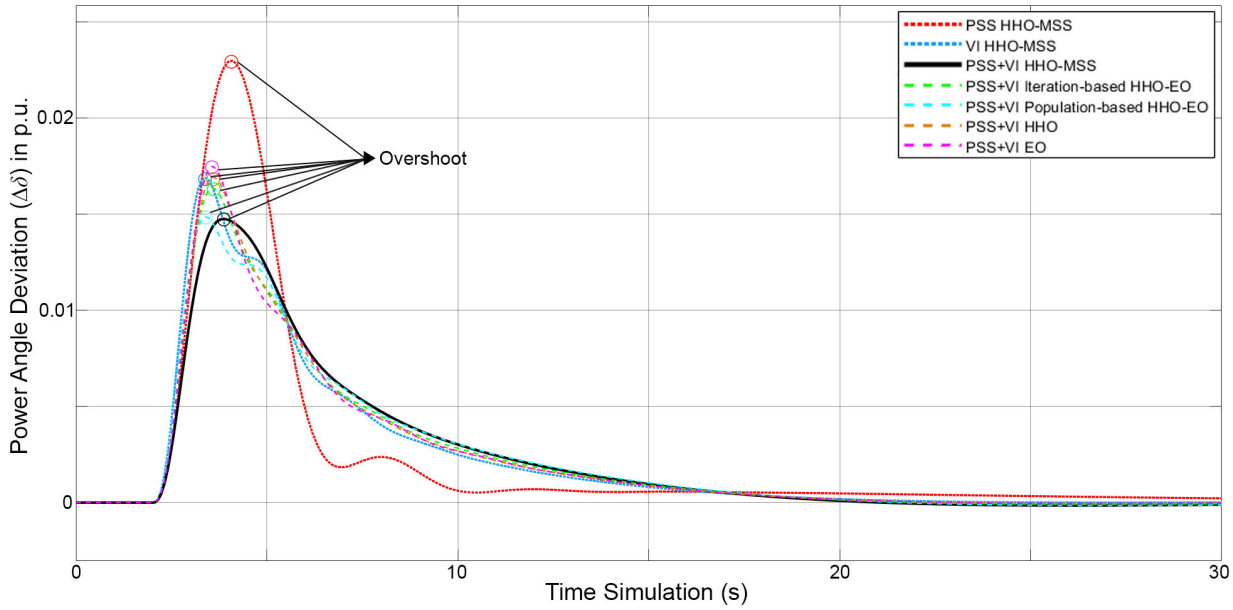

FIGURE 21. $\Delta\delta$ response in full-RES penetration with PSS and VI.

TABLE 19. Detailed response in full-RES penetration with PSS and VI.

Parameter	Method						
	PSS HHO-MSS	VI HHO-MSS	PSS+VI HHO-MSS	PSS+VI Iter-based HHO-EO	PSS+VI Pop-based HHO-EO	PSS+VI HHO	PSS+VI EO
Freq. nadir (%)	-0.111	-0.115	-0.079	-0.098	-0.099	-0.1	-0.104
Δf Overshoot (p.u.)	5.3×10^{-4}	-1.22×10^{-4}	2.07×10^{-4}	2.12×10^{-4}	-1.79×10^{-4}	2.17×10^{-4}	2.23×10^{-4}
Δf Settling time (s)	10.036	9.449	9.126	9.045	7.989	9.25	9.3
$\Delta\delta$ Overshoot (p.u.)	2.29×10^{-2}	1.69×10^{-2}	1.47×10^{-2}	1.64×10^{-2}	1.48×10^{-2}	1.69×10^{-2}	1.75×10^{-2}
$\Delta\delta$ Settling time (s)	8.61	11.002	11.384	11.454	11.635	11.968	12.114

On the other hand, the VI becomes more impactful. The optimal parameters of PSS and VI by HHO-MSS give the best improvement in reducing frequency nadir of 46.47% from the base case, which is followed by PSS+VI Iteration-based HHO-EO, Population-based HHO-EO, HHO, and EO of 43.53%, 40.59%, 27.05%, and 22.35%, respectively.

HHO-MSS gives the smoothest dampening effect in high-RES penetration. It can be indicated in the overshoot response that several methods (VI HHO-MSS, PSS+VI Iteration-based HHO-EO, and PSS+VI Population-based HHO-EO) have an overdamped effect (first overshoot is lower than steady state point), and the other ones are underdamped. It indicates that several methods are less able to adapt in different cases. The Δf improvement is also correlated with $\Delta\delta$. It can be observed that a higher RES penetration gives more power angle deviation reduction. It means a higher RES penetration gives more ability to maintain δ to its reference point after a disturbance occurs. The analysis shows that the PSS and VI by HHO-MSS have the best ability to improve dynamic stability in high-RES penetration.

6) TIME DOMAIN SIMULATION: FULL-RES SCENARIO

In full-RES penetration, the Δf and $\Delta\delta$ responses with PSS and VI are shown in Figure 20 and Figure 21. The detailed response is given in Table 19. The characteristics of this condition are similar to high-RES ones. The PSS is no longer effective in maintaining dynamic stability. Although the frequency nadir reduction with PSS is similar to VI, the PSS cannot dampen the oscillation like VI. The PSS and VI have reduced frequency nadir by 34.70% and 32.35%, respectively. Furthermore, the optimal parameters of PSS and VI by HHO-MSS offer the best frequency nadir improvement of 53.52%, followed by Iteration-based HHO-EO, Population-based HHO-EO, HHO, and EO of 42.35%, 41.76%, 41.17%, and 38.82%, respectively.

TABLE 20. Performance index validation on Δf response.

Performance Index	Base	PSS HHO-MSS	VI HHO-MSS	PSS+VI HHO-MSS	PSS+VI Iter-based HHO-EO	PSS+VI Pop-based HHO-EO	PSS+VI HHO	PSS+VI EO
		Error reduction (-%)						
Low-RES Penetration								
IAE	5.53×10^{-3}	34.38	18.01	34.05	34.03	34.52	34.45	34.92
ITAE	5.04×10^{-2}	16.98	14.60	13.00	12.50	12.60	12.80	16.37
ISE	3.62×10^{-6}	65.75	27.68	71.13	70.72	67.29	67.60	63.70
ITSE	1.51×10^{-5}	60.76	43.64	62.22	61.73	59.32	59.79	58.48
Avg. reduction (-%)		44.47	25.98	45.10	44.74	43.43	43.66	43.37
Mid-RES Penetration								
IAE	4.73×10^{-3}	21.82	39.34	40.06	39.94	40.95	40.76	38.35
ITAE	3.3×10^{-2}	14.00	20.27	14.48	13.27	14.39	14.30	11.45
ISE	3.54×10^{-6}	51.36	70.65	75.48	75.88	73.70	73.10	76.66
ITSE	1.37×10^{-5}	49.12	69.85	72.56	72.44	71.61	71.30	71.20
Avg. reduction (-%)		34.07	50.03	50.65	50.38	50.16	49.86	49.42
High-RES Penetration								
IAE	4.56×10^{-3}	22.06	35.20	37.15	35.99	37.68	33.33	31.67
ITAE	2.8×10^{-2}	17.79	9.79	4.93	6.50	4.21	18.25	19.29
ISE	3.65×10^{-6}	42.49	68.47	74.60	73.67	74.27	58.22	53.67
ITSE	1.41×10^{-5}	45.96	68.50	72.62	71.45	72.72	60.24	56.79
Avg. reduction (-%)		32.07	45.49	47.32	46.90	47.22	42.51	40.35
Full-RES Penetration								
IAE	4.97×10^{-3}	12.07	30.40	31.53	33.04	32.76	33.46	32.41
ITAE	3.55×10^{-2}	4.23	5.86	8.82	2.73	4.42	6.31	5.35
ISE	3.9×10^{-6}	43.49	67.18	74.96	73.46	71.31	68.79	69.90
ITSE	1.56×10^{-5}	38.06	64.69	68.64	69.40	67.34	65.65	66.20
Avg. reduction (-%)		24.46	42.03	45.99	44.66	43.96	43.55	43.47
Overall avg. reduction (-%)		33.76	40.88	47.26	46.67	46.19	44.89	44.15

The HHO-MSS has also offered dynamic stability improvement with the best dampening effect to the Δf and $\Delta\delta$ responses resulting in the smoothest overshoot. Although the smooth responses expense a bit longer settling time, it can be tolerated. Unlike the other method that has overdamped or underdamped responses. Moreover, with very high-RES penetration, $\Delta\delta$ can be maintained at its reference point after a disturbance occurs. Thus, it can be concluded that HHO-MSS has the best capability in conducting the optimal parameters of PSS and VI in various RES conditions.

7) PERFORMANCE INDEX VALIDATION

The appropriateness of the modified objective function based on the Benson Scalarization Technique is validated using performance indexes: Integral Absolute Error (IAE), Integral Time Absolute Error (ITAE), Integral Squared Error (ISE), and Integral Time Squared Error (ITSE). The Δf response validation is given in Table 20. The performance index calculation is performed within 50-s time simulation.

It can be seen from Table 20 that all of the methods have decent error reduction. It means that the proposed approach by combining the damping factor and damping ratio by the Benson Scalarization Technique is appropriate to be applied. Moreover, the performance index validation is correlated to eigenvalue and time domain simulation analysis. First, the optimal parameters by HHO-MSS have the best overall average error reduction of 47.26%. It is followed by Iteration-based HHO-EO and Population-based HHO-EO which have similar results of 46.67% and 46.19%, respectively. Then, the HHO and EO have also similar error reductions of 44.89% and 44.15%, respectively. Second, PSS has better error reduction than VI in low-RES penetration. However, VI has conducted better results in the other scenarios than PSS. The performance index validation concludes that the optimal configuration by HHO-MSS is superior to the others.

V. CONCLUSION

This paper has presented a new approach for controlling the parameters of PSS and VI to improve the dynamic stability of the renewable microgrid. A new HHO-MSS is proposed. Various RES penetration conditions are simulated to represent the behavior of renewable microgrids with conventional generators, PVES, WTES, and BESS. The Benson Scalarization Technique is introduced to combine two objective functions based on damping factor and damping ratio. The proposed algorithm has been compared to the other modified

algorithms based on HHO and EO, HHO, and EO. Using the Friedman Ranking Test, HHO-MSS has conducted a superior improvement in exploration and exploitation ability. Based on the convergence curve and energy escaping curves analysis, it can be seen that HHO-MSS has a more balanced proportion than basic HHO in the exploration and exploitation process.

In the controlling parameters of PSS and VI cases, the HHO-MSS conducts 9.63% to 26.57% better fitness value based on f_{benson} than the compared algorithms. HHO-MSS gives the most appropriate dynamic stability performance based on eigenvalue analysis. Furthermore, in time domain simulation analysis conducted in low, mid, high, and full RES penetrations, HHO-MSS offers the best improvement in frequency nadir, reducing overshoot, and refining the Δf and $\Delta\delta$ responses. From the eigenvalue analysis and time domain simulation, it can be concluded that PSS gives better stability improvement in low and mid RES penetrations, while VI gives better stability improvement in high and full RES penetrations. The proposed approach by controlling parameters of PSS and VI by HHO-MSS in a hybrid approach gives the best stability improvement in all RES penetrations. The performance indexes validate the optimal configuration approach by combining the damping factor and damping ratio by Benson Scalarization is appropriate to be applied. Moreover, the PSS and VI by HHO-MSS have the best overall average error reduction of 47.26%.

In future work, the proposed approach will be implemented in more complex power systems with more detailed working conditions. Now, this paper is focused on microgrid power systems. In the future, interconnected power systems or multi-area power systems or large-scale power systems can be considered as study cases. Besides that, detailed working conditions such as intermittency and fluctuation of RES conditions, system faults, and other external factors can be included.

ACKNOWLEDGMENT

The authors would like to be grateful to the Indonesian Government for the PMDSU Batch VI and PKPI 2023 scholarship programs. This research was conducted in collaboration with the Power System Operation and Control (PSOC) Laboratory, Department of Electrical Engineering, Institut Teknologi Sepuluh Nopember (ITS), and Dr. Ryo Nishimura's Laboratory, Faculty of Engineering, Tottori University.

REFERENCES

[1] M. Uddin, H. Mo, D. Dong, S. Elsawah, J. Zhu, and J. M. Guerrero, "Microgrids: A review, outstanding issues and future trends," *Energy Strategy Rev.*, vol. 49, Sep. 2023, Art. no. 101127, doi: 10.1016/j.esr.2023.101127.

[2] M. A. Prakasa and S. Subiyanto, "Optimal cost and feasible design for grid-connected microgrid on campus area using the robust-intelligence method," *Clean Energy*, vol. 2021, pp. 823–840, 2022.

[3] M. Elgendi, M. AlMallahi, A. Abdelkhalig, and M. Y. E. Selim, "A review of wind turbines in complex terrain," *Int. J. Thermofluids*, vol. 17, Feb. 2023, Art. no. 100289, doi: 10.1016/j.ijft.2023.100289.

[4] T. Kerdphol, F. S. Rahman, M. Watanabe, and Y. Mitani. (2021). *Virtual Inertia Synthesis and Control*. [Online]. Available: https://link.springer.com/book/10.1007/978-3-030-57961-6

[5] J. Machowski, Z. Lubosny, J. Bialek, and J. Bumby, *Power System Dynamics: Stability and Control*. Hoboken, NJ, USA: Wiley, 2020.

[6] P. S. Kundur and O. P. Malik, *Power System Stability and Control*, 2nd ed. New York, NY, USA: McGraw-Hill, 2022.

[7] A. Nocoń and S. Paszek, "A comprehensive review of power system stabilizers," *Energies*, vol. 16, no. 4, p. 1945, Feb. 2023, doi: 10.3390/en16041945.

[8] M. A. Prakasa and I. Robandi, "Tuning improvement of power system stabilizer using hybrid Harris hawk optimization-equilibrium optimizer algorithm," in *Proc. 6th Int. Conf. Inf. Technol., Inf. Syst. Electr. Eng. (ICITISEE)*, Dec. 2022, pp. 553–558.

[9] T. Kerdphol, F. S. Rahman, Y. Mitani, M. Watanabe, and S. K. Küfeoglu, "Robust virtual inertia control of an islanded microgrid considering high penetration of renewable energy," *IEEE Access*, vol. 6, pp. 625–636, 2018, doi: 10.1109/ACCESS.2017.2773486.

[10] A. Pratap, S. K. Sharma, and A. Khandelwal, "A review of modern virtual inertia control strategies for microgrid implementation," in *Proc. IEEE 2nd Int. Conf. Electr. Power Energy Syst. (ICEPES)*, Dec. 2021, pp. 1–6, doi: 10.1109/ICEPES52894.2021.9699804.

[11] S. Impram, S. Varbak Nese, and B. Oral, "Challenges of renewable energy penetration on power system flexibility: A survey," *Energy Strategy Rev.*, vol. 31, Sep. 2020, Art. no. 100539, doi: 10.1016/j.esr.2020.100539.

[12] P. Jaengarun, S. Tiptipakorn, and T. Singhavilai, "Comparative study of PSS and POD for a power system with PV plant," in *Proc. Int. Conf. Power, Energy Innov. (ICPEI)*, Oct. 2020, pp. 169–172, doi: 10.1109/ICPEI49860.2020.9431424.

[13] P. He, Q. Fang, H. Jin, Y. Ji, Z. Gong, and J. Dong, "Coordinated design of PSS and STATCOM-POD based on the GA-PSO algorithm to improve the stability of wind-PV-thermal-bundled power system," *Int. J. Electr. Power Energy Syst.*, vol. 141, Oct. 2022, Art. no. 108208, doi: 10.1016/j.ijepes.2022.108208.

[14] J. Bhukya and V. Mahajan, "Optimization of damping controller for PSS and SSSC to improve stability of interconnected system with DFIG based wind farm," *Int. J. Electr. Power Energy Syst.*, vol. 108, pp. 314–335, Jun. 2019, doi: 10.1016/j.ijepes.2019.01.017.

[15] M. R. Djalal, I. Robandi, and M. A. Prakasa, "Stability enhancement of sulselrabar electricity system using mayfly algorithm based on static var compensator and multi-band power system stabilizer PSS2B," *IEEE Access*, vol. 11, pp. 57319–57340, 2023, doi: 10.1109/ACCESS.2023.3283598.

[16] L. Yathisha and S. Patilkulkarni, "LQR and LQG based optimal switching techniques for PSS and UPFC in power systems," *Control Theory Technol.*, vol. 16, no. 1, pp. 25–37, Feb. 2018, doi: 10.1007/s11768-018-6174-x.

[17] U. Markovic, Z. Chu, P. Aristidou, and G. Hug, "Fast frequency control scheme through adaptive virtual inertia emulation," in *Proc. IEEE Innov. Smart Grid Technol. Asia (ISGT Asia)*, May 2018, pp. 787–792, doi: 10.1109/ISGT-Asia.2018.8467920.

[18] A. Faragalla, O. Abdel-Rahim, M. Orabi, and E. H. Abdelhameed, "Enhanced virtual inertia control for microgrids with high-penetration renewables based on whale optimization," *Energies*, vol. 15, no. 23, p. 9254, Dec. 2022, doi: 10.3390/en15239254.

[19] A. Mohamed, H. Elzoghby, M. Bahgat, and A. G. Mohamed, "Enhanced non-linear PID-based on virtual inertia control to enhance the frequency stability of a hybrid power system," *Int. J. Adv. Eng. Bus. Sci.*, vol. 3, no. 3, pp. 1–18, Aug. 2022, doi: 10.21608/ijaebs.2022.155614.1029.

[20] J. Ansari, A. R. Abbasi, M. H. Heydari, and Z. Avazzadeh, "Simultaneous design of fuzzy PSS and fuzzy STATCOM controllers for power system stability enhancement," *Alexandria Eng. J.*, vol. 61, no. 4, pp. 2841–2850, Apr. 2022, doi: 10.1016/j.aej.2021.08.007.

[21] Q. Li, B. Ren, Q. Li, D. Wang, W. Tang, J. Meng, and X. Wu, "Virtual inertial control strategy based on fuzzy logic algorithm for PMSG wind turbines to enhance frequency stability," *Frontiers Energy Res.*, vol. 10, pp. 1–9, May 2022, doi: 10.3389/fenrg.2022.907770.

[22] V. Skiparev, J. Belikov, E. Petlenkov, and Y. Levron, "Reinforcement learning based MIMO controller for virtual inertia control in isolated microgrids," in *Proc. IEEE PES Innov. Smart Grid Technol. Conf. Eur. (ISGT-Europe)*, Oct. 2022, pp. 1–5, doi: 10.1109/ISGT-Europe54678.2022.9960447.

[23] A. Oshnoei, O. Sadeghian, B. Mohammadi-Ivatloo, F. Blaabjerg, and A. Anvari-Moghaddam, "Data-driven coordinated control of AVR and PSS in power systems: A deep reinforcement learning method," in *Proc. IEEE Int. Conf. Environ. Electr. Eng. IEEE Ind. Commercial Power Syst. Eur.*, Sep. 2021, pp. 1–6, doi: 10.1109/EEEIC/ICPSEurope51590.2021.9584640.

[24] G. Zhang, W. Hu, J. Zhao, D. Cao, Z. Chen, and F. Blaabjerg, "A novel deep reinforcement learning enabled multi-band PSS for multi-mode oscillation control," *IEEE Trans. Power Syst.*, vol. 36, no. 4, pp. 3794–3797, Jul. 2021, doi: 10.1109/TPWRS.2021.3067208.

[25] M. Nasir, M. Saloumi, and A. B. Nassif, "Review of various metaheuristics techniques for tuning parameters of PID/FOPID controllers," in *Proc. ITM Web Conf.*, vol. 43, 2022, p. 01002, doi: 10.1051/itmconf/20224301002.

[26] M. E. C. Bento, D. Dotta, R. Kuiava, and R. A. Ramos, "A procedure to design fault-tolerant wide-area damping controllers," *IEEE Access*, vol. 6, pp. 23383–23405, 2018, doi: 10.1109/ACCESS.2018.2828609.

[27] E. V. Fortes, L. F. B. Martins, M. V. S. Costa, L. Carvalho, L. H. Macedo, and R. Romero, "Mayfly optimization algorithm applied to the design of PSS and SSSC-POD controllers for damping low-frequency oscillations in power systems," *Int. Trans. Electr. Energy Syst.*, vol. 2022, pp. 1–23, Apr. 2022.

[28] M. A. El-Dabah, M. H. Hassan, S. Kamel, and H. M. Zawbaa, "Robust parameters tuning of different power system stabilizers using a quantum artificial gorilla troops optimizer," *IEEE Access*, vol. 10, pp. 82560–82579, 2022, doi: 10.1109/ACCESS.2022.3195892.

[29] M. Almas Prakasa and I. Robandi, "Optimal tuning for power system stabilizer using arithmetic optimizer algorithm in interconnected two-area power system," in *Proc. Int. Seminar Intell. Technol. Appl. (ISITIA)*, Jul. 2023, pp. 798–803, doi: 10.1109/ISITIA59021.2023.10221034.

[30] M. A. Prakasa and I. Robandi, "Power system stabilizer tuning improvement for single-machine infinite bus using equilibrium optimizer algorithm," in *Proc. Int. Semin. Intell. Technol. Appl.*, Jul. 2022, pp. 320–352, doi: 10.1109/ISITIA56226.2022.9855203.

[31] A. Toolabi Moghadam, M. Aghahadi, M. Eslami, S. Rashidi, B. Arandian, and S. Nikolovski, "Adaptive rat swarm optimization for optimum tuning of SVC and PSS in a power system," *Int. Trans. Electr. Energy Syst.*, vol. 2022, pp. 1–13, Jan. 2022, doi: 10.1155/2022/4798029.

[32] R. K. Khadanga, D. Das, A. Kumar, and S. Panda, "Sine augmented scaled arithmetic optimization algorithm for frequency regulation of a virtual inertia control based microgrid," *ISA Trans.*, vol. 138, pp. 534–545, Jul. 2023, doi: 10.1016/j.isatra.2023.02.025.

[33] K. Hongesombut and R. Keteruksa, "Fractional order based on a flower pollination algorithm PID controller and virtual inertia control for microgrid frequency stabilization," *Electric Power Syst. Res.*, vol. 220, Jul. 2023, Art. no. 109381, doi: 10.1016/j.epsr.2023.109381.

[34] M. Shehab, I. Mashal, Z. Momani, M. K. Y. Shambour, A. AL-Badareen, S. Al-Dabet, N. Bataina, A. R. Alsoud, and L. Abualigah, "Harris hawks optimization algorithm: Variants and applications," *Arch. Comput. Methods Eng.*, vol. 29, no. 7, pp. 5579–5603, Nov. 2022, doi: 10.1007/s11831-022-09780-1.

[35] A. A. Heidari, S. Mirjalili, H. Faris, I. Aljarah, M. Mafarja, and H. Chen, "Harris hawks optimization: Algorithm and applications," *Future Gener. Comput. Syst.*, vol. 97, pp. 849–872, Aug. 2019, doi: 10.1016/j.future.2019.02.028.

[36] H. M. Ridha, A. A. Heidari, M. Wang, and H. Chen, "Boosted mutation-based Harris hawks optimizer for parameters identification of single-diode solar cell models," *Energy Convers. Manage.*, vol. 209, Apr. 2020, Art. no. 112660, doi: 10.1016/j.enconman.2020.112660.

[37] Y. Wei, H. Lv, M. Chen, M. Wang, A. A. Heidari, H. Chen, and C. Li, "Predicting entrepreneurial intention of students: An extreme learning machine with Gaussian barebone Harris hawks optimizer," *IEEE Access*, vol. 8, pp. 76841–76855, 2020, doi: 10.1109/ACCESS.2020.2982796.

[38] H. Jia, C. Lang, D. Oliva, W. Song, and X. Peng, "Dynamic Harris hawks optimization with mutation mechanism for satellite image segmentation," *Remote Sens.*, vol. 11, no. 12, p. 1421, Jun. 2019, doi: 10.3390/rs11121421.

[39] E. H. Houssein, M. E. Hosney, D. Oliva, W. M. Mohamed, and M. Hassaballah, "A novel hybrid Harris hawks optimization and support vector machines for drug design and discovery," *Comput. Chem. Eng.*, vol. 133, Feb. 2020, Art. no. 106656, doi: 10.1016/j.compchemeng.2019.106656.

[40] S. Ekinci, D. Izci, and B. Hekimoglu, "PID speed control of DC motor using Harris hawks optimization algorithm," in *Proc. Int. Conf. Electr., Commun., Comput. Eng. (ICECCE)*, Jun. 2020, pp. 1–6, doi: 10.1109/ICECCE49384.2020.9179308.

[41] D. Izci and S. Ekinci, "An efficient FOPID controller design for vehicle cruise control system using HHO algorithm," in *Proc. 3rd Int. Congr. Hum.-Comput. Interact., Optim. Robotic Appl. (HORA)*, Jun. 2021, pp. 1–5, doi: 10.1109/HORA52670.2021.9461336.

[42] D. Izci, S. Ekinci, A. Demirören, and J. Hedley, "HHO algorithm based PID controller design for aircraft pitch angle control system," in *Proc. Int. Congr. Hum.-Comput. Interact., Optim. Robotic Appl.*, Jun. 2020, pp. 1–6, doi: 10.1109/HORA49412.2020.9152897.

[43] H. Gezici and H. Livatyall, "Chaotic Harris hawks optimization algorithm," *J. Comput. Design Eng.*, vol. 9, no. 1, pp. 216–245, Feb. 2022, doi: 10.1093/jcde/qwab082.

[44] M. Song, H. Jia, L. Abualigah, Q. Liu, Z. Lin, D. Wu, and M. Altalhi, "Modified Harris hawks optimization algorithm with exploration factor and random walk strategy," *Comput. Intell. Neurosci.*, vol. 2022, pp. 1–23, Apr. 2022.

[45] B. K. Tripathy, P. K. Reddy Maddikunta, Q.-V. Pham, T. R. Gadekallu, K. Dev, S. Pandya, and B. M. ElHalawany, "Harris hawk optimization: A survey on variants and applications," *Comput. Intell. Neurosci.*, vol. 2022, pp. 1–20, Jun. 2022, doi: 10.1155/2022/2218594.

[46] A. Faramarzi, M. Heidarinejad, B. Stephens, and S. Mirjalili, "Equilibrium optimizer: A novel optimization algorithm," *Knowl.-Based Syst.*, vol. 191, Mar. 2020, Art. no. 105190, doi: 10.1016/j.knosys.2019.105190.

[47] L. Chaib, A. Choucha, S. Arif, H. G. Zaini, A. El-Fergany, and S. S. M. Ghoneim, "Robust design of power system stabilizers using improved Harris hawk optimizer for interconnected power system," *Sustainability*, vol. 13, no. 21, p. 11776, Oct. 2021, doi: 10.3390/su132111776.

[48] A. N. A. Maulidhia, D. A. Asfani, A. Priyadi, and H. Setiadi, "Frequency stability analysis on optimization of virtual inertia control (VIC) capacitor energy storage (CES) controller settings using particle swarm optimization," in *Proc. Int. Conf. Comput. Eng., Netw., Intell. Multimedia (CENIM)*, Nov. 2022, pp. 359–364, doi: 10.1109/CENIM56801.2022.10037313.

[49] B. N. Syifa, D. A. Asfani, A. Priyadi, and H. Setiadi, "Frequency stability analysis on optimization of virtual inertia controller settings based on retired electric vehicles battery using firefly algorithm," in *Proc. Int. Conf. Comput. Eng., Netw., Intell. Multimedia (CENIM)*, Nov. 2022, pp. 1–6, doi: 10.1109/CENIM56801.2022.10037414.

[50] I. Robandi, *Modern Power System Control*. Jakarta, Indonesia: Penerbit, 2009.

[51] J. Ritonja, M. Petrun, J. Cernelic, R. Brezovnik, and B. Polajzer, "Analysis and applicability of heffron–phillips model," *Elektronika Ir Elektrotechnika*, vol. 22, no. 4, pp. 3–10, Aug. 2016, doi: 10.5755/j01.eie.22.4.15905.

[52] A. A. Sallam and O. P. Malik, *Power System Stability: Modelling, Analysis and Control*. London, England: The Institution of Engineering and Technology, 2015.

[53] T. Kerdphol, F. S. Rahman, M. Watanabe, Y. Mitani, D. Turschner, and H.-P. Beck, "Enhanced virtual inertia control based on derivative technique to emulate simultaneous inertia and damping properties for microgrid frequency regulation," *IEEE Access*, vol. 7, pp. 14422–14433, 2019, doi: 10.1109/ACCESS.2019.2892747.

[54] D.-J. Lee and L. Wang, "Small-signal stability analysis of an autonomous hybrid renewable energy power generation/energy storage system Part I: Time-domain simulations," *IEEE Trans. Energy Convers.*, vol. 23, no. 1, pp. 311–320, Mar. 2008, doi: 10.1109/TEC.2007.914309.

[55] T. Kerdphol, K. Fuji, Y. Mitani, M. Watanabe, and Y. Qudaih, "Optimization of a battery energy storage system using particle swarm optimization for stand-alone microgrids," *Int. J. Electr. Power Energy Syst.*, vol. 81, pp. 32–39, Oct. 2016, doi: 10.1016/j.ijepes.2016.02.006.

[56] *IEEE Recommended Practice for Excitation System Models for Power System Stability Studies*, IEEE, Piscataway, NJ, USA, 2016.

[57] Z. I. E. Cicek and Z. K. Ozturk, "A comparative study of scalarization techniques on the multi-objective single machine-scheduling problem under sequence-dependent setup time, release date and due date constraints," *Gazi Univ. J. Sci.*, vol. 33, no. 2, pp. 429–444, Jun. 2020, doi: 10.35378/gujs.581780.

[58] I. Çetinbas, B. Tamyürek, and M. Demirtas, "Sizing optimization and design of an autonomous AC microgrid for commercial loads using Harris hawks optimization algorithm," *Energy Convers. Manage.*, vol. 245, Oct. 2021, Art. no. 114562, doi: 10.1016/j.enconman.2021.114562.

MOHAMAD ALMAS PRAKASA was born in Brebes, in September 1999. He received the bachelor's degree from the Department of Electrical Engineering, Universitas Negeri Semarang (UNNES), Semarang, Indonesia, in 2017, and the master's degree from the Department of Electrical Engineering, Institut Teknologi Sepuluh Nopember (ITS), Surabaya, Indonesia, in 2021, where he is currently pursuing the Ph.D. degree with a Fast-Track Scholarship Program from the PMDSU Scholarship Program, Indonesia. He is a member of the Power System Operation and Control (PSOC) Laboratory. His research interests include artificial intelligence application to electrical power systems, especially to dynamic stability and RES microgrid optimization.

IMAM ROBANDI was born in Kebumen, in August 1963. He received the bachelor's degree from the Department of Electrical Engineering, Institut Teknologi Sepuluh Nopember (ITS), Surabaya, Indonesia, in 1989, the master's degree from the Department of Electrical Engineering, Institut Teknologi Bandung (ITB), Bandung, Indonesia, in 1995, and the Ph.D. degree from the Department of Electrical Engineering, Tottori University, Japan, in 2002. He is currently a Professor with the Department of Electrical Engineering, ITS. He is also the Head of the Power System Operation and Control (PSOC) Laboratory. His research interests include artificial intelligence applications for large-scale electrical and energy power systems.

RYO NISHIMURA was born in Sapporo, Japan, in July 1966. He received the bachelor's, master's, and Ph.D. degrees from the Department of Nuclear Engineering, Hokkaido University, Japan, in 1989, 1991, and 1994, respectively. He is currently an Associate Professor with the Department of Electrical Engineering and Computer Science, Tottori University. His research interests include heuristic algorithms, PV power generation, and the application of electrostatics.

MUHAMMAD RUSWANDI DJALAL was born in Ujung Pandang, in March 1990. He received the bachelor's degree in energy engineering from Politeknik Negeri Ujung Pandang, Makassar, Indonesia, in 2012, and the master's degree from the Department of Electrical Engineering, Institut Teknologi Sepuluh Nopember (ITS), Surabaya, Indonesia, in 2015. He is currently pursuing the Ph.D. degree with the Department of Electrical Engineering, ITS. He is a Lecturer in energy engineering with the Department of Mechanical Engineering, Politeknik Negeri Ujung Pandang. His research interests include power system stability, renewable energy, and artificial intelligence.